HAL
open science

Silver in geological fluids from in situ X-ray absorption spectroscopy and first-principles molecular dynamics

Gleb S. Pokrovski, Jacques Roux, Guillaume Ferlat, Romain Jonchiere, Ari P. Seitsonen, Rodolphe Vuilleumier, Jean-Louis Hazemann

To cite this version:

Gleb S. Pokrovski, Jacques Roux, Guillaume Ferlat, Romain Jonchiere, Ari P. Seitsonen, et al.. Silver in geological fluids from in situ X-ray absorption spectroscopy and first-principles molecular dynamics. Geochimica et Cosmochimica Acta, 2013, 106, pp.501-523. 10.1016/j.gca.2012.12.012 . hal-00794819

HAL Id: hal-00794819

https://hal.science/hal-00794819v1

Submitted on 12 Sep 2020

HAL is a multi-disciplinary open access archive for the deposit and dissemination of scientific research documents, whether they are published or not. The documents may come from teaching and research institutions in France or abroad, or from public or private research centers.

L'archive ouverte pluridisciplinaire **HAL**, est destinée au dépôt et à la diffusion de documents scientifiques de niveau recherche, publiés ou non, émanant des établissements d'enseignement et de recherche français ou étrangers, des laboratoires publics ou privés.

University of Zurich[UZH]

Zurich Open Repository and Archive
University of Zurich
Main Library
Strickhofstrasse 39
CH-8057 Zurich
www.zora.uzh.ch

Year: 2013

Silver in geological fluids from in situ X-ray absorption spectroscopy and first-principles molecular dynamics

Pokrovski, Gleb S ; Roux, Jacques ; Ferlat, Guillaume ; Jonchiere, Romain ; Seitsonen, Ari P ; Vuilleumier, Rodolphe ; Hazemann, Jean-Louis

DOI: https://doi.org/10.1016/j.gca.2012.12.012

Posted at the Zurich Open Repository and Archive, University of Zurich
ZORA URL: https://doi.org/10.5167/uzh-81918
Journal Article
Accepted Version

Originally published at:
Pokrovski, Gleb S; Roux, Jacques; Ferlat, Guillaume; Jonchiere, Romain; Seitsonen, Ari P; Vuilleumier, Rodolphe; Hazemann, Jean-Louis (2013). Silver in geological fluids from in situ X-ray absorption spectroscopy and first-principles molecular dynamics. Geochimica et Cosmochimica Acta, 106:501-523.
DOI: https://doi.org/10.1016/j.gca.2012.12.012

Silver in geological fluids from in situ X-ray absorption spectroscopy and first-principles molecular dynamics

Gleb S. Pokrovski [1]*, Jacques Roux [2], Guillaume Ferlat [3], Romain Jonchiere [3,5], Ari P. Seitsonen [4], Rodolphe Vuilleumier [5], Jean-Louis Hazemann [6]

1- Géosciences Environnement Toulouse (GET, ex-LMTG), Observatoire Midi-Pyrénées, Université de Toulouse, CNRS, IRD, 14 avenue Edouard Belin, F-31400 Toulouse, France

2- Equipe PMM, Institut de Physique du Globe de Paris, 4 Place Jussieu, F-75252 Paris cedex 05, France

3- IMPMC, Institut de Minéralogie et de Physique des Milieux Condensés, Université P. & M. Curie (UPMC), UMR CNRS-UPM C-IPGP 7590, 4, Place Jussieu, F-75252 Paris cedex 05, France.

4- Physikalisch-Chemisches Institut der Universität Zürich, Winterthurerstrasse 190, CH-8057, Zurich Switzerland.

5- Département de Chimie, Ecole Normale Supérieure, UMR CNRS-ENS-UPMC 8640, 24 rue Lhomond, F-75231 Paris, France.

6- Institut Néel, CNRS, 25 avenue des Martyrs, F-38042 Grenoble Cedex 9, France

* Corresponding author:
phone: (33)-(0)5-61-33-26-18; fax: (33)-(0)5-61-33-25-60;
e-mail: gleb.pokrovski@get.obs-mip.fr

Running title: Silver in hydrothermal fluids

Keywords: silver; chloride; hydrothermal fluid; X-ray absorption spectroscopy; Ag-Cl complexes; molecular dynamics; XANES; EXAFS; thermodynamic properties; ore deposits

Revised version # GCA-D-12-00383 for Geochimica et Cosmochimica Acta

November 2012

ABSTRACT

The molecular structure and stability of species formed by silver in aqueous saline solutions typical of hydrothermal settings were quantified using in situ X-ray absorption spectroscopy (XAS) measurements, quantum-chemical modeling of near-edge absorption spectra (XANES) and extended fine structure spectra (EXAFS), and first-principles molecular dynamics (FPMD). Results show that in nitrate-bearing acidic solutions to at least 200°C, silver speciation is dominated by the hydrated Ag^+ cation surrounded by 4 to 6 water molecules in its nearest coordination shell with mean Ag-O distances of ~2.32±0.02 Å. In NaCl-bearing acidic aqueous solutions of total Cl concentration from 0.7 to 5.9 mol/kg H_2O (m) at temperatures from 200 to 450°C and pressures to 750 bar, the dominant species are the di-chloride complex $AgCl_2^-$ with Ag-Cl distances of 2.40±0.02 Å and Cl-Ag-Cl angle of 160±10°, and the tri-chloride complex $AgCl_3^{2-}$ of a triangular structure and mean Ag-Cl distances of 2.55±0.05 Å. With increasing temperature, the contribution of the tri-chloride species decreases from ~50% of total dissolved Ag in the most concentrated solution (5.9m Cl) at 200°C to less than 10-20% at supercritical temperatures for all investigated solutions, so that $AgCl_2^-$ becomes by far the dominant Ag-bearing species at conditions typical of hydrothermal-magmatic fluids. Both di- and tri-chloride species exhibit outer-sphere interactions with the solvent as shown by the detection, using FPMD modeling, of H_2O, Cl^-, and Na^+ at distances of 3 to 4 Å from the silver atom. The species fractions derived from XAS and FPMD analyses, and total $AgCl_{(s)}$ solubilities, measured in situ in this work from the absorption edge height of XAS spectra, are in accord with thermodynamic predictions using the stability constants of $AgCl_2^-$ and $AgCl_3^{2-}$ from Akinfiev and Zotov (2001) and Zotov et al. (1995), respectively, which are based on extensive previous AgCl(s) solubility measurements. These data are thus recommended for chemical equilibrium calculations in mineral-fluid systems above 200°C. In contrast, our data disagree with SUPCRT-based datasets for Ag-Cl species, which predict large fractions of high-order chloride species, $AgCl_3^{2-}$ and $AgCl_4^{3-}$ in high-temperature saline fluids. Comparisons of the structural and stability data of Ag-Cl species derived in this study with those of their Au and Cu analogs suggest that molecular-level differences amongst the chloride complexes such as geometry, dipole moment, distances, and resulting outer-sphere interactions with the solvent may account, at least partly, for the observed partitioning of Au, Ag and Cu in vapor-brine and fluid-melt systems. In hydrothermal environments dominated by fluid-rock interactions, the contrasting affinity of these metals for sulfur ligands and the differences both in chemistry and stability of their main solid phases (Ag sulfides, Cu-Fe sulfides, and native Au) largely control the concentration and distribution of these metals in their economic deposits.

1. INTRODUCTION

There is a growing need for better understanding the silver behavior in hydrothermal systems hosting a major part of Ag resources on Earth. Despite the low abundance of silver in the continental crust (~50 ppb, Rudnick and Gao, 2003), this trace element is enriched in hydrothermal fluids, with concentrations up to ~100 ppm in brines as show fluid-inclusion analyses (e.g., Heinrich et al., 1999; Ulrich et al., 1999; Audétat et al., 2000; Borisova et al., 2012). Although silver usually follows its geochemical analogs, copper and gold, Ag/Cu and Ag/Au ratios in magmatic-hydrothermal deposits vary over 3-4 orders of magnitude. For example, typical Ag/Au mass ratios in porphyry deposits and epithermal adularia-quartz and alunite-quartz deposits, ~1÷1000, are significantly higher than those of Carlin-type, skarn, and orogenic gold deposits, ~0.001÷1 (e.g., Sillitoe and Hedenquist, 2003; Pal'yanova, 2008). Silver also fractionates from gold and copper in vapor-brine systems of magmatic-hydrothermal settings, where Ag partitions preferentially into the saline solution, whereas Au and Cu often enrich the aqueous low-density vapor, as inferred from natural fluid inclusion data and laboratory experiments (Pokrovski et al., 2005a, 2008a; Kouzmanov and Pokrovski, 2012; references therein). Knowledge of the chemical speciation of silver in geological fluids over the range of magmatic-hydrothermal conditions is the primary requisite for modeling Ag transfers in natural vapor-fluid-melt systems, identifying favorable conditions of Ag-bearing minerals formation, and interpreting Ag tenors in different types of deposits. The present contribution is aimed to provide new data on the stoichiometry and structure of aqueous complexes that carry silver in hydrothermal fluids.

Among the three major natural ligands, hydroxide, sulfide, and chloride that transport base and precious metals in saline liquids and vapors, the Cl^- ion is believed to be the principal carrier of Ag, similarly to other base metals (Fe, Zn, Pb), as demonstrated by numerous experimental studies of Ag-bearing mineral solubilities and vapor-liquid and fluid-melt partitioning (e.g., Wood et al., 1987; Zotov et al., 1995; Wood and Samson, 1998; Pokrovski et al., 2005a, 2008a,b; Simon et al., 2008; references therein). The other two ligands, H_2S/HS^- and H_2O/OH^-, may contribute to Ag solubility only in fluids

characterized by low temperatures and salinities, alkaline pH and/or elevated sulfide contents (e.g., Webster, 1986; Stefánsson and Seward, 2003; references therein). The effect of less common ligands such as ammonia (e.g., Wood and Samson, 1998), selenide (Akinfiev et al., 2008), bromide and iodide (Gammons and Yu, 1997), which may form strong chemical bonds with the Ag^+ ion, is expected to be weak in typical hydrothermal fluids with low concentrations of these components compared to the far more abundant chloride.

There is thus little doubt that chloride complexes play the major role in the hydrothermal and magmatic transport of Ag; however, they have been a subject of rather limited experimental work concerning the exact stoichiometry and thermodynamic stability of these important species. Two major sources of data on Ag-Cl aqueous species are those of Seward (1976) and Zotov et al. (1995, references therein) who carried out systematic measurements of native silver (Ag) and chlorargirite (AgCl) solubility over wide temperature (T), pressure (P) (to 450°C and 1.5 kbar) and Cl concentration (to 7 m NaCl and/or KCl) ranges. Their data indicate that the dichloride $AgCl_2^-$ is likely to be the dominant species to at least 2m Cl; the mono-chloride complex $AgCl^0$ is significant only in dilute solutions (< 0.01m Cl); higher-order chloride complexes ($AgCl_3^{2-}$) form only in concentrated Cl brines at moderate temperatures. The large stability of $AgCl_2^-$ was confirmed by subsequent solubility work conducted in narrower T-P-composition windows (e.g., Gammons and Williams-Jones, 1995; Akinfiev and Zotov, 1999). Because the thermodynamic properties of the crystalline silver chloride, $AgCl_{(s)}$, and aqueous $AgCl_2^-$ were believed to be well constrained at T $\leq$ 300°C from those works, they were used indirectly to derive the formation constants of aqueous HCl^0 and chloride complexes of a number of metals like Zn, Ca, Mn, Pt, Pd, Nd by measuring changes in AgCl(s) solubility in the presence of the metal cation in moderately-saline solutions (Ruaya and Seward, 1986, 1987; Williams-Jones and Seward, 1989; Gammons, 1995; Gammons and Seward, 1996; Gammons et al., 1996; Tagirov et al., 1997).

However, large discrepancies exist on both stability and stoichiometry of Ag-Cl complexes at elevated salt concentrations (> 2m) typical of natural magmatic-hydrothermal fluids. In particular, tri- and

tetra-chloride complexes, which are known for silver at ambient temperatures (Martell et al., 2004,) and for many other metals (Fe, Pb, Zn, Cd) both at ambient and hydrothermal conditions (e.g., Wood and Samson, 1998; Martell et al., 2004; Testemale et al., 2009; Bazarkina et al., 2010; references therein), were insufficiently explored for Ag above 100-200°C. Based on the available solubility studies cited above and ambient-temperature data on [$AgCl_{1-4}$] complexes from abundant chemical literature (Martell et al., 2004, NIST Critical database 8.0; refs therein), Sverjensky et al. (1997) and Akinfiev and Zotov (2001) have generated two independent datasets of thermodynamic properties of Ag-Cl complexes using the revised Helgeson-Kirkham-Flowers (HKF) model (Tanger and Helgeson, 1988). These datasets are now integrated in computer codes and largely used by geochemists; however, they appear surprisingly inconsistent as shown in Fig. 1. Calculations using these two datasets reveal large differences at T > 300°C and m_{Cl} > 1.5m in the Ag chloride species distribution dominated either by $AgCl_2^-$ (Akinfiev and Zotov, 2001) or $AgCl_4^{3-}$ (Sverjensky et al., 1997). This leads to large discrepancies when predicting Ag-bearing minerals solubility in saline fluids at elevated T, attaining a factor of 10 to 100 in dissolved Ag concentration above 400°C over the acidity and sulfur fugacity ranges typical of natural fluids (Fig. 2). These discrepancies may also affect the thermodynamic data for other metal chloride complexes derived from solubility measurements of AgCl(s) (see above). In addition to the chloride number (also commonly referred to as ligation number), knowledge of species geometry and hydration structure (i.e., presence of water molecules in the Ag coordination shell) is also required to interpret Ag partitioning in brine-vapor systems (Pokrovski et al., 2005a, 2008a). Molecular structures of Ag species are necessary to make sound physical-chemical comparisons with its analogues, Au and Cu, which also form chloride complexes in hydrothermal fluids.

In situ X-ray absorption spectroscopy (XAS) provides a direct way to resolve the discrepancies of the Ag-Cl species stoichiometry and to access their structures and hydration numbers. In contrast to its analogs Au and Cu whose major chloride and sulfide complexes in high T-P aqueous solution have recently been investigated using XAS (Fulton et al., 2000; Brugger et al., 2007, Berry et al., 2009;

Pokrovski et al., 2009a,b; Etschmann et al., 2010), the only data available for Ag at T above ambient is a XAS study of Ag^+ hydration to 300°C and saturated vapor pressure (P_{sat}) are those of Seward et al. (1996). This cation is however unlikely to play a major role in typical chloride-bearing fluids (see above). Recent improvements in the design of high T-P optical cells for synchrotron (e.g., Testemale et al., 2005) allow now in situ XAS measurements on dissolved metals to supercritical conditions, avoiding the difficulties of classical hydrothermal-reactor techniques related to bulk solubility determination (e.g., artifacts related to sampling or quenching, Pokrovski et al., 2008b) and its interpretation in terms of dissolved species (e.g., choice of speciation models based on bulk solubility, Pokrovski et al., 2006). In addition, a far more rigorous analysis of XAS data is now possible owing to the progress in quantum-chemistry and molecular dynamics modeling allowing robust constraints on electronic structures, species geometries, hydration shells, and solute-solvent interactions (e.g., Ferlat et al., 2002; Dang et al., 2006; D'Angelo et al., 2008; Sherman, 2010).

In this work, we performed in situ XAS measurements (including near-edge structure spectra or XANES, and extended fine structure or EXAFS spectra) on silver chloride aqueous solutions in a wide salinity range (0.7-5.9m Cl) at 200-450°C and 600-800 bar. The data were processed using classical EXAFS analyses, quantum-chemical simulations of XANES, and first-principles molecular dynamics modeling of Ag-Cl-H_2O interactions in aqueous solution. Results provide new speciation and structural data on Ag chloride complexes responsible for the transport of this metal by geological fluids, and allow a better interpretation of the behavior of Ag and associated metals (Au and Cu) in hydrothermal settings.

2. MATERIALS AND METHODS

2.1. Experimental design and X-ray absorption spectra acquisition

XAS measurements were performed on one nitrate $AgNO_3$-HNO_3 and three chloride AgCl-NaCl-HCl aqueous solutions, prepared from analytical grade reagents and deionized water. Solution compositions are reported in Table 1 in molality units (m = number of moles of each solute per kg of water). Hydrogen peroxide (0.05-0.10 m

H_2O_2) was also added in each solution to prevent precipitation of native silver that may happen at elevated temperature (e.g., Seward, 1973). A weighed amount of silver chloride, which is weakly soluble at ambient temperature (< 0.001m), was pressed in pellets and loaded in the experimental cell. Total dissolved silver concentration in solution was measured from the absorption edge height in transmission mode (Pokrovski et al., 2005b, 2009a; Table 1). The solubility of $AgCl_{(s)}$ increases with temperature (e.g., Seward, 1976), and the acquisition was started $\geq$ 200°C when dissolved Ag concentrations are high enough ($\geq$ 0.01 m) to allow low-noise EXAFS spectra to be obtained in transmission mode (see below). At moderate T (200-300°C), dissolved Ag concentrations attain a steady state value within 10 min. after the temperature reach and remain stable for at least several hours, indicating that equilibrium with AgCl(s) is likely to be reached. The rapid equilibrium reach is in agreement with previous batch-reactor solubility studies (Seward, 1976; Zotov et al., 1995). However, at T > 300°C and high salinities with large excess of solid phase, Ag dissolved concentrations decreased systematically and $AgCl_{(s)}$ precipitation occurred on the colder optical windows of the cell at the X-ray beam passage. This was manifested by noisy spectra clearly showing the contribution of the solid whose spectrum is very different from those of solutions. In the experiments reported in this study, this was carefully avoided by using smaller amounts of $AgCl_{(s)}$, corresponding to under-saturated solutions at T > 300°C. In this case, spectra from solutions show no detectable contribution of $AgCl_{(s)}$. Thus, AgCl(s) solubility could only be accurately measured at 200°C for all Cl concentrations and at 300°C for the lowest m_{Cl} concentration (0.7m, Table 1). Although minor losses of Ag from solution owing to $AgCl_{(s)}$ precipitation in the colder zones of the cell, close to the pistons which are out of the sample space probed by X-rays, were still observed for some experiments above 300°C (Table 1), it did not affect the XAS spectra from solution, demonstrating that no precipitation of $AgCl_{(s)}$ occurs at the beam passage.

XAS spectra from Ag aqueous solutions were collected at the Ag K-edge (~25.5 keV) over the energy range 25.2-26.7 keV on BM29 bending-magnet beamline (Filipponi et al., 2000) at the European Synchrotron Radiation Facility (ESRF, Grenoble, France). The storage ring was operated at 6 GeV with a ~200 mA current. The beam energy was selected using a Si (311) double-crystal monochromator detuned by 30% to eliminate higher-order harmonics. Energy was calibrated using a silver metal foil and setting the maximum of its main-edge spectrum derivative at 25.514 keV. Spectra were recorded in transmission mode using ion chambers filled with Ar gas. Multiple XAS scans were performed on each T-P-composition point, with an acquisition time of ~40 min/scan. Experiments were conducted using a high T-P cell developed at the Institute Néel (Grenoble) and recently

described in detail elsewhere (Pokrovski et al., 2005b, 2006, 2009a; Testemale et al., 2005). Both solution and solid were placed in the internal cell that consists of a vertical 1-mm thick glassy-carbon tube and two coaxial sapphire pistons, which delimit the sample space and move in the tube in response to T-P changes. The cell is heated by electrical resistances and placed in a stainless-steel vessel pressurized with helium gas and equipped with beryllium windows for X-ray passage. Temperature in the sample space was controlled within ±5°C by thermocouples attached to the glassy-carbon tube. Pressure was monitored by manometers at the cell exit and the end of pressure line; pressure differences between them do not exceed a few bars.

2.2. X-ray absorption spectra analysis

EXAFS data analysis was performed with the HORAE and IFEFFIT programs (Ravel and Newville, 2005) and following the recommendations of the International XAFS Society (Sayers, 2000). Details about the reduction procedure can be found elsewhere for similar metals (Pokrovski et al., 2006, 2009a,b). Briefly, energies were recalculated into k-space ($Å^{-1}$) with E_0 (i.e., the energy at which k is zero) chosen as the maximum of the first derivative of the main-edge spectrum. Spectra were normalized to the absorption edge height, background removed, weighted by k^n, where n = 1, 2 and 3, and Fourier transformed (FT) over the k range 3.0-11.6 $Å^{-1}$ for chloride and 3.0-10.0 $Å^{-1}$ for nitrate aqueous samples. The shorter k-range for nitrate solutions is dictated by i) the low amplitude of the Ag-O EXAFS signal at high k-values comparable to the spectral noise, and ii) the presence of multielectron excitations $KM_{4,5}$ and $KM_{2,3}$ that appear in the chi(k) data at 10.3 and 12.7 $Å^{-1}$ (Fulton et al., 2009). In contrast, the EXAFS spectrum of the Ag-Cl contribution dominant in Cl-bearing solutions has a higher signal-to-noise ratio above 10 $Å^{-1}$ and thus is much less affected by the multielectron transitions. This was checked by EXAFS fits of larger k-ranges (up to 13.5 $Å^{-1}$) for some low-noise spectra; they yielded no changes within errors in the derived structural parameters. Fits were performed in R-space on both real and imaginary parts of the FT contributions to obtain the identity of neighbor atoms, Ag-neighbor distance (R), coordination number (N), and Debye-Waller factor (σ^2) for each scattering path (Table 1). A single nonstructural parameter Δe was varied to account for the difference between the experimental absorption-edge energy and its estimate made by FEFF. To diminish correlations between N and σ^2, and better account for light (O) versus heavy (Cl) neighbors and multiple scattering paths, fits were performed simultaneously with k-weighting of 1, 2 and 3. The fitted values of structural parameters were identical within errors, with comparable fit qualities at each k-weighting. This is an additional demonstration of

both the validity of the chosen structural models and the accuracy of the EXAFS background removal procedure (Ravel and Newville, 2005; Kelly et al., 2008). Theoretical backscattering amplitude and phase-shift functions for Ag-O and Ag-Cl single and multiple scattering paths were computed by the FEFF6 ab-initio code (Zabinsky et al., 1995) using $AgNO_3$ and AgCl crystal structures (Gibbons and Trotter, 1971; Hull and Keen, 1999). The amplitude reduction factor (S_0^2) was set at 0.75±0.05 as found by fitting the spectra of crystalline Ag_2O, $AgNO_3$, AgCl, and Ag_2S solids. The effect of inharmonic disorder was accounted using the cumulant expansion method with third- and fourth-order cumulant~~s~~ (c_3 and c_4). Multiple scattering (MS) events within the Ag first coordination shell were tested using the FEFF code, assuming tetrahedral, trigonal pyramidal, and linear geometries around Ag as found in the model compounds.

In addition to classical EXAFS analyses, XANES spectra of different Ag-Cl-H_2O molecular clusters were modeled ab-initio based on the experimental EXAFS-derived Ag-Cl and Ag-O distances and geometries found from molecular dynamics (see below) using the FDMNES computer code (Joly, 2001). Details about this approach for aqueous species can be found elsewhere (e.g., Testemale et al., 2004; Pokrovski et al., 2009a, Bazarkina et al., 2010). Very briefly, calculations of theoretical XANES spectra of different cluster's symmetry and geometry were performed using the Finite Difference Method (FDM) with an energy resolution of < 0.1 eV (note that in case of low symmetry, the muffin-tin approximation is not sufficient in the near-edge energy range; Joly, 2001). The obtained spectra, which display almost all possible electronic transitions, are further convoluted with a Lorentzian function with a full width of 6.75 eV (Gamma_hole key in the FDMNES input file) to account for the core-hole lifetime at the Ag K-edge, and a Gaussian function to account for the experimental resolution assumed to be equal to the intrinsic resolution of the (311) monochromator (1.1 eV). The value of energy of the Fermi level (E_{fermi}) was fixed to -3.0 eV based on the examination of the density of states (DOS) of the different electronic levels. Changing the values of E_{fermi} from -6 to 0 eV produces only minor effects on the calculated XANES spectra.

2.3. First-principles molecular dynamics simulations

Three different compositions in the model Ag-NaCl-H_2O system were simulated, each consisting of 128 water molecules, 1 Ag^+, 1 Na^+, and 2, 3 or 4 Cl^- ions. These numbers of Cl^- ions correspond to apparent Cl molalities (m_{Cl}) of 0.9, 1.3, and 1.7, respectively, but because of the low Cl/Ag ratios in our systems (from 2 to 4), the concentration of free Cl^- not complexed with Ag is much smaller. This should be kept in mind when comparing

253 the FPMD results with XAS data from experimental Ag-Na-Cl solutions, where total Cl/Ag ratios are much higher
254 (from 20 to 100, Table 1). The model with 4 Cl^- ions was examined at near-ambient (50°C, 1 bar) and supercritical
255 (380°C, 600 bar) conditions. The models with 2 and 3 Cl^- ions were simulated at supercritical conditions only.

256 The stability of Cl^--bearing complexes was simulated by inserting pre-formed $AgCl_n^{(n-1)-}$ clusters with n = 2
257 to 4. For n = 4, the initial geometric configuration is a tethahedral complex with Ag-Cl bonds of 2.35 Å and Cl-Ag-
258 Cl angles of 109.5°. For n = 3 and n = 2, the initial configurations were derived from the latter one by removing
259 chlorine atoms. To accelerate the equilibration of the surrounding water molecules, classical molecular dynamics
260 simulations using empirical force-fields were ran for typically 1 ns while keeping fixed the geometry of the $AgCl_n^{(n-}$
261 $^{1)-}$ complexes. Cubic periodic boundary conditions were employed. The box sizes were adjusted to reach a pressure
262 value close to the target pressures in the empirical force-field simulations (1 bar at 50°C and 600 bar at 380°C),
263 while being guided by the equation of state of the NaCl-H_2O system (Anderko and Pitzer, 1993; Bakker, 2003). The
264 resulting cubic box sizes are 15.7 Å and 17.8 Å for the system with 4 Cl^- at near-ambient and supercritical
265 conditions, respectively, and 18.0 Å and 17.7 Å for the systems with 2 and 3 Cl^-, respectively. The final
266 configurations obtained at the end of the classical runs were then used as starting configurations for FPMD
267 simulations.

268 The FPMD simulations were carried out within the Density Functional Theory (DFT) framework and
269 the Born-Oppenheimer method using the freely available program package QUICKSTEP/CP2K (VandeVondele et
270 al., 2005a). QUICKSTEP uses a hybrid Gaussian plane-wave (GPW) method (Lippert et al. 1997). A triple-zeta
271 valence doubly polarized (TZV2P) basis set was chosen for oxygen, hydrogen, and chlorine (VandeVondele et al.
272 2005b), whereas the double-zeta valence plus polarization (DZVP) basis set optimized for molecules
273 (VandeVondele et al., 2007) was employed for silver. Core electrons were replaced by the Goedecker-Teter-Hutter
274 (GTH) norm-conserving pseudo-potentials (Goedecker et al., 1996; Hartwigsen et al., 1998; Krack, 2005). A
275 neutralizing background charge was implicitly added for all charged systems. The cutoff for the electronic density
276 was set to a high converged value, 600 Ry, with smoothing for the exchange-correlation contribution
277 (VandeVondele et al., 2005a). The gradient-corrected exchange-correlation functional BLYP (Becke, 1998; Lee et
278 al., 1998) was used in the DFT calculations. This functional is known to provide accurate structural results, e.g.
279 inter-atomic distances are over-estimated by only 1-2% (Sprik et al., 1996). Van der Waals interactions were taken
280 into account using the scheme of Grimme (2006). Constant temperature conditions were imposed by a Nosé-

Hoover thermostat chain (Nosé 1984a,b). The time step for the MD simulations was 0.5 fs. The simulations were run for 100 ps at 50°C and for 50 ps at 380°C.

MD-EXAFS spectra were calculated from the FPMD trajectories using the FEFF code (Zabinsky et al., 1995) and the methodology detailed in Ferlat et al. (2005). Spherical clusters of a radius of 8 Å centered at the silver atom were extracted every 5 fs, providing a total of 20,000 clusters at 50°C and 10,000 clusters at 380°C. An individual EXAFS signal for each cluster was generated including all the contributions from multiple-scattering paths up to 6 legs. In these calculations, the amplitude reduction factor (S_0^2) was set to 0.75 as obtained experimentally, leaving a single parameter Δe to match the experimental and calculated energy mesh. The scattering potentials were calculated in the muffun-tin approximation, and it has been checked that use of the ab-initio self-consistent field scheme led to almost identical results.

3. RESULTS

3.1. Analysis of EXAFS spectra

3.1.1. Nitrate solutions

EXAFS spectra of a Cl-free silver nitrate solution (exp #1, 0.21m $AgNO_3$-0.10m HNO_3-0.10m H_2O_2), in which the hydrated Ag^+ cation is dominant, could only be acquired to 200°C, because of the rapid loss of dissolved Ag from solution above that temperature due to the precipitation of native silver, likely caused by the reducing environment of the glassy-carbon cell and/or beam-induced effects common for redox-sensitive metals (e.g., Pokrovski et al., 2009a). The spectra collected at 30, 100, and 200°C (Fig. 3), display a single contribution from the first-shell oxygen neighbors without any clearly detectable outer-shell signal or multiple scattering paths. The spectra show both reduction in chi(k) and FT magnitudes and shift to shorter Ag-O distances with increasing temperature (Fig. 3). This is confirmed by quantitative EXAFS modeling yielding Ag-O average distances from 2.34 to 2.30 Å and number of oxygen neighbors from ~6 to ~4.5 when T increases from 30 to 200°C, whereas DW factors of the Ag-O shell remain constant within errors (Table 1). Neither significant anharmonic effects as approximated by

the third- and fourth-order cumulants ($c_3 < 3\times10^{-4}$, $c_4 < 5\times10^{-5}$), nor presence of two different Ag-O distances were detected within the spectral resolution.

The absolute values of R and DW parameters derived in this study are identical within errors to those reported by Seward et al. (1996) using EXAFS spectroscopy for similar nitrate solutions from 20 to 300°C at saturated vapor pressure (P_{sat}). Our Ag-O distances at near-ambient temperature, R_O=2.34±0.02 Å, compare favorably with previous ambient-temperature studies of the aqua Ag^+ ion by EXAFS (Yamaguchi et al., 1984a), X-ray and neutron diffraction (Yamagushi et al., 1984b; Sandstrom et al., 1985; Skipper and Neilson, 1989), and large angle X-ray scattering (LAXS, Persson and Nilsson, 2006). Most of these studies report Ag-O coordination numbers around four at ambient conditions, which is consistent with the tetrahedral $Ag(H_2O)_4^+$ cation, also suggested from UV spectroscopy (Texter et al., 1983) and theoretical DFT quantum chemistry and molecular dynamics (MD) simulations (e.g., Martinez et al., 1997; Feller et al., 1999; Bernasconi et al., 2004). However, other MD simulations (e.g., Armunanto et al., 2003; Fulton et al., 2009) and recent analyses of Ag L- and K-edge EXAFS spectra of silver perchlorate and nitrate solutions (Fulton et al., 2009) are less categorical about the tetrahedral Ag^+ geometry, rather suggesting a five- or six-coordinated Ag^+ in aqueous solution. Although our EXAFS-derived coordination numbers are closer to these values (~5-6 O atoms, Table 1), they exhibit significant errors (±1.5 atoms at least). We believe that the issue of the Ag^+-H_2O coordination cannot be resolved on the solely base of EXAFS data, but it will require independent information from XANES spectra, which are more sensitive to the cluster geometry and symmetry, as will be shown in section 3.2. Molecular dynamics simulations of Ag^+ in Cl-free aqueous solution will be presented in a subsequent paper.

3.1.2. Chloride solutions

EXAFS spectra and their Fourier transform magnitudes of the three studied Ag chloride solutions of 0.7, 2.6 and 5.9m total Cl are plotted in Fig. 3a,b. They are different both in phase and amplitude from those of the Ag-O environment in nitrate solution, suggesting the predominance of heavier

backscatterrers, presumably Cl. Qualitative continuous Cauchy wavelet transforms analyses (CCWT, Munoz et al., 2003) demonstrate that the EXAFS is dominated by the Ag nearest shell composed of Cl atoms without any detectable presence of other types of atoms like O (electronic annex EA-1). No outer-shell neighbors or multiple scattering signals are detectable within the spectral resolution (Fig. 3b, EA1-1). In particular, all analyzed spectra show no detectable contribution from $AgCl_{(s)}$ that might precipitate at the beam passage (see section 2.1). The spectra from solution are devoid of all features typical of the AgCl solid (strong Ag-Ag contributions in EXAFS, particular shape and magnitude of XANES, and large N and R values, see below). The EXAFS spectra of chloride solutions reveal weak but clearly identifiable variations in both phase and amplitude for the same Cl concentration with T change, and amongst different Cl solutions at a given T, suggesting that the Ag-Cl atomic environment depends on both T and m_{Cl}.

This is confirmed by quantitative EXAFS fits (Table 1, electronic annex EA-2), which show that average Ag-Cl distances for concentrated chloride solutions systematically decrease over a range of ~0.05-0.07 Å with increasing T (e.g., from 2.49 Å at 200°C to 2.42 Å at 450°C for the 5.9m Cl solution; Fig. 4A). At the same T, the Ag-Cl distance increases slightly with increasing Cl concentration (e.g., from 2.38 to 2.44 Å at 400°C/600 bar, when m_{Cl} increases from 0.7 to 5.9m; Fig. 4A). The trend in average number of Cl atoms around Ag (N_{Cl}) is less clear, showing values of 2.0±0.2 atoms at T $\geq$ 300°C in the whole m_{Cl} range (Fig. 4B). At lower T, N_{Cl} values are somewhat higher, attaining ~2.5 for the most concentrated solution (5.9m Cl at 200°C). Note however, that the precise evolution of N_{Cl} with T and salinity may be hidden inside the high intrinsic uncertainties associated with this EXAFS parameter. The DW factors of the Ag-Cl shell (σ^2) do not show significant T trends for any investigated solution, but are systematically higher on average at higher m_{Cl} (e.g., differences attain a factor of 2 between the most dilute and most concentrated solution, despite similar N_{Cl}, see Table 1). In addition to the three major structural parameters above, significant anharmonic disorder in Ag-Cl distances was detected as expressed by the c_3 cumulant (Table 1). Despite large intrinsic uncertainties associated with this

parameter (±50% of the value itself), its inclusion in the model, particularly for the most concentrated solution, yielded a 2- to 3-fold improvement in fit quality as compared with cumulant-free fits. A rough tendency for the c_3 parameter is a slight decrease with increasing T and decreasing m_{Cl} (with the exception of the 5.9m Cl sample at 200°C, Table 1). The derived EXAFS parameters are distinct from those of the AgCl solid (R_{Cl} ~2.8 Å, N_{Cl} = 6; Hull and Keen, 1999) implying a different Ag coordination environment in aqueous chloride solutions.

To the best of our knowledge, this study is the first measurement of the molecular structure of aqueous silver chloride complexes. Our derived Ag-Cl coordination numbers (N_{Cl} = 1.8÷2.5) and inter-atomic distances (R_{Cl} = 2.37÷2.49 Å) are significantly smaller than those in crystalline (N_{Cl} = 6, R_{Cl} ~ 2.8 Å at 25°C) and molten (N_{Cl} = 3÷4, R_{Cl} ~ 2.6 Å at 500÷800°C) silver chloride (e.g., Inui et al., 1991; Kawakita et al., 2007). In most inorganic and organic compounds with O/N/Cl/P/S ligands, Ag(I) exhibits a distorted tetrahedral coordination with Ag-Cl distances of 2.5÷2.7 Å (ICSD database, 2010), which are at least 0.1-0.2 Å longer than those of this study. The shorter distances found in solution are in agreement with lower Ag coordination numbers and the absence of first-shell water molecules in aqueous Ag chloride complexes compared to most Ag-bearing solids. Our Ag-Cl distances are in agreement with those predicted by DFT modeling of di- and tri-coordinated Ag-Cl-H_2O clusters (Godinho et al., 2005). The structural parameters derived in our study imply the likely predominance of di-chloride complexes in aqueous solution with some fraction, at low T, of complexes having higher Cl numbers. It is, however, important to note that despite the close Cl coordination numbers found for all solutions at $\geq$ 300°C, Ag-Cl distances and DW factors increase systematically with increasing Cl content. This may suggest the simultaneous presence of different [$AgCl_2$] geometries and/or the presence, in concentrated saline solutions, of outer Cl^- and Na^+ ions that affect first-shell distances and disorder but are beyond direct detection by EXAFS. Principal component analyses (PCA, Malinowski, 1991); Rossberg et al., 2003) of the investigated EXAFS spectra of Cl solutions indicate two factors necessary to describe the experimental dataset. Although this might further support the presence of two kinds of species in the

experimental solutions, PCA on T- and m_{Cl}-series of EXAFS spectra for aqueous complexes may be biased by i) the smoothness of changes in metal-ligand distance and ligation number with Cl content, which leads to the lack of contrast and consequent underestimation of the number of species (e.g., Bazarkina et al., 2010), and ii) changes in metal-ligand distance and disorder with T for the same species, which may overestimate the number of species. Following these limitations of EXAFS and PCA, independent approaches are necessary to better constrain the species stoichiometry and geometry, as shown in the next sections by analyses of XANES spectra and molecular dynamics modeling.

3.2. Quantum-chemical modeling of XANES spectra

Normalized XANES spectra of selected nitrate and chloride solutions are plotted in Fig. 5a. The nitrate samples are characterized by slightly higher absorption edge energies (by ~1 eV, defined as the maximum of 1st derivative of the spectrum) and more pronounced white-line amplitudes (feature A in Fig. 5a) at ~25,525 eV (~1.1×absorption step) than the chloride samples (~0.9×absorption jump). Temperature changes in the nitrate spectra are manifested by a slight decrease of the white-line amplitude, likely reflecting the decrease in the Ag-O coordination number as found from the EXAFS analyses above, and also confirmed by XANES modeling below. XANES spectra of chloride solutions have weakly pronounced white-line amplitudes typical for di-coordinated Cu(I) and Au(I) chloride and sulfide complexes (e.g., Brugger et al., 2007; Pokrovski et al., 2009a,b; Etschmann et al., 2010). The second after-edge resonance at ~25,545±3 eV of chloride spectra (feature B in Fig. 5a) is in opposite phase with that of nitrate spectra, in agreement with the change of Ag-O to Ag-Cl environment in saline solutions. Spectra of chloride solutions exhibit small but systematic shifts of the white line low-energy side by 1-2 eV towards higher energy with increasing T and decreasing m_{Cl}, which results in narrowing of the white-line width, as exemplified by spectra of 0.7m Cl at 450°C and 5.9m Cl at 200°C in Fig. 5a. All other spectra at intermediate m_{Cl} and T fit in between these two 'end members'. Neither the spectra of nitrate nor chloride samples resemble those of $AgNO_{3(s)}$ and $AgCl_{(s)}$ reference compounds having, respectively, a

distorted AgO_7 (Gibbons and Trotter, 1971) and a regular octahedral $AgCl_6$ (Hull and Keen, 1999) geometry. This suggests a different coordination environment of Ag in aqueous solution.

In the absence of adequate references for aqueous samples, the interpretation of their XANES spectra is greatly helped by quantum-chemical modeling. Theoretical XANES spectra of $[AgO_mCl_n]$ clusters of different geometry (from linear to octahedral, with variable degree of distortion) and stoichiometry ($0 \leq (m, n) \leq 6$) were calculated using the FDMNES program (Joly, 2001) and the experimental Ag-O and Ag-Cl distances from EXAFS and/or FPMD calculations (section 3.3). Variations in these distances within 0.1 Å as found by EXAFS (section 3.1, Fig. 4) yield only minor changes in the width and amplitude of calculated XANES features, without altering significantly the shapes and energy positions of the main resonances. The effect of H atoms (as water molecules or free protons) and outer-sphere Na/Cl atoms (with Ag-Na and Ag-Cl distances > 3 Å) on the calculated spectra was found to be too weak to affect their major features and was thus neglected. Note that the low sensitivity of calculated XANES spectra to all these parameters is due to the poor intrinsic resolution imposed by the large core-hole life time of the electron at Ag K-edge (~7 eV), so that only major changes of geometry and ligand identity in the Ag nearest shell could be unambiguously identified.

Calculated XANES spectra of representative types of Ag-O-Cl clusters are shown in Fig. 5b. Three main features are apparent in this figure. a) The white line (feature A) around 25,525 eV is higher in energy (by 1-2 eV) and amplitude (10-30%) for Ag-O clusters compared with Ag-Cl clusters of same stoichiometries. Its amplitude generally grows from linear or angular $AgCl_2$ and AgO_2 to tetrahedral-like AgO_4 and $AgCl_4$ clusters. Octahedral-like AgO_6 and $AgCl_6$ clusters have spectral shapes different from their tetrahedral counterparts, with white lines of narrower width and smaller amplitude. b) The second resonance (feature B) at ~25540 eV in $[AgCl_{2\text{-}4}]$ clusters is in opposite phase with that of their $[AgO_{2\text{-}4}]$ analogs. Features A and B are very similar to those observed in the experimental spectra of nitrate and chloride solutions (Fig. 5a). c) A shoulder (feature C) appears at ~25533 eV for mixed AgO/Cl clusters, reflecting the presence of both types of atoms around Ag. This feature is not observed in our experimental

Cl solutions; this corroborates the absence of O atoms in the first coordination shell of Ag as deduced from EXAFS analyses (section 3.1) and wavelet transforms (EA-1). The similarity of experimental spectra of Cl solutions with those calculated for low Cl number clusters (Fig. 5a, b) suggests that Ag speciation in our saline solutions is likely to be dominated by di- and tri-chloride species, which is also in line with the EXAFS-derived average Cl numbers (Table 1).

Experimental spectra of silver nitrate and chloride solids and silver nitrate solution are compared with FDMNES calculated spectra for selected clusters of different geometries in Fig. EA3. Note a similarity between measured and calculated XANES for $AgCl_{(s)}$ and $AgNO_{3(s)}$ compounds (Fig. EA3-1); this further supports the validity of the modeling. Experimental XANES spectra of Ag nitrate solutions are closest to those predicted for tetrahedral-like AgO_4 clusters (Fig. EA3-1), in good agreement with most available literature data (see section 3.1) and our molecular dynamics modeling (which will be reported in a future contribution), suggesting the tetrahedral-like hydrated $Ag(H_2O)_4^+$. Moderate distortions in Ag-O distances (~0.1 Å) and symmetry of $Ag(H_2O)_4^+$ from a regular tetrahedron as identified by this and some previous studies could not however be confirmed unambiguously by XANES modeling owing to the insufficient spectral resolution at the Ag K-edge.

Experimental spectra of the two most contrasting chloride solutions (0.7m Cl at 450°C and 5.9m Cl at 200°C) are compared with those of representative Ag-Cl clusters in Fig. 6. XANES spectra from the low-concentrated chloride solution (0.7m Cl) at 400 and 450°C resemble most closely those of the $[AgCl_2]$ cluster with ClAgCl angles around 150-160° (Fig. 6a). A linear $AgCl_2$ geometry (∠ClAgCl = 180°) yields white-line shapes somewhat steeper and sharper than the experimental spectrum. Furthermore, a linear geometry of the Cl-Ag-Cl bonds would produce significant multiple scattering (MS) contributions in EXAFS spectra, as indicated by FEFF calculations of this study and observed for the quasi-linear di-chloride complexes $Cu(I)Cl_2^-$ (∠ClCuCl $\geq$ 160°C, Brugger et al., 2007) and linear $Au(I)Cl_2^-$ (Pokrovski et al., 2009b). Our EXAFS spectra do not show such MS features (Fig. 3b), implying a bend geometry, in better agreement with the XANES results. Angles ClAgCl $\leq$ 120° of the

[$AgCl_2$] cluster yield too flat white-line resonances to be compatible with experimental spectra (Fig. 6a). The experimental spectrum of the most concentrated Cl solution at the lowest T (5.9m Cl, 200°C) has a shape between those predicted for a [$AgCl_2$] cluster with a ClAgCl angle of 150° and a trigonal pyramidal or plane [$AgCl_3$] cluster with ∠ClAgCl between 120 and 100° (Fig. 6b). A better geometry resolution within a given Ag:Cl stoichiometry is not achievable from our XANES spectra at the Ag K-edge. In contrast, tetra-coordinated [$AgCl_4$] clusters yield spectra with narrower and more intense white lines, yielding less satisfactory match of the experimental spectra.

This analysis indicates that moderately concentrated solutions are likely to be dominated by the di-chloride complex, $AgCl_2^-$, in agreement with the EXAFS-derived Cl numbers of 2, whereas the most concentrated solutions at low-T contain a mixture of di and tri-coordinated Ag-Cl complexes, which is also consistent with the EXAFS-derived Cl numbers of ~2.5 for experiment #5 of 5.9m Cl at 200°C (Table 1). All other solutions at intermediate T and/or m_{Cl} fall in between these XANES shapes. A deeper insight into the species geometry and solvation environment is provided by molecular dynamics as discussed below.

3.3. First-principles molecular dynamics simulations

The FPMD simulations starting from initial cluster geometries (see section 2.3) were ran for times long enough to visualize the cluster reorganization, i.e. exchange of H_2O molecules and Cl atoms in the nearest Ag environment. Analyses of MD trajectories (e.g., Fig. EA4-1) allow different silver-chlorine complexes to be identified, depending on T and m_{Cl}. The stable complexes found are shown in Fig. 7. Radial and angular distribution functions for these complexes were extracted from subsets of the FPMD trajectories (e.g., Fig. 8 for $AgCl_2^-$).

At the near-ambient temperature (50°C), several different species persist along our 100 ps trajectory: $AgCl_4^{3-}$, $AgCl_3(H_2O)^{2-}$, $AgCl_3^{2-}$, and $AgCl_2^-$ (see Fig. EA4-3). In all these complexes, the chlorine atoms form a well-defined first coordination shell around Ag, well separated from the subsequent

water hydration shells (e.g., Fig. 8a). The closest shell of water molecules is found at ~3.5 Å from the silver atom at all temperatures; more distant hydration shells cannot be clearly distinguished (Fig. 8a), reflecting the looseness of such long Ag-H_2O bonds and dynamic nature of solute-solvent interactions. Outer shell water molecules at distances above 3 Å from the metal atom were also reported using MD simulations for Cu di-chloride (Sherman, 2007) and Au hydrogensulfide (Liu et al., 2011) complexes. All along the simulation, the Na^+ ion is found far away, i.e. at least 6 Å, from the silver atom (Fig. EA4-3). The $AgCl_4^{3-}$ complex is a highly distorted tetrahedron with two Cl atoms at an average Ag-Cl distance of 2.44 Å, and the two other Cl atoms being at a much larger distance from Ag (3.48 Å). The species $AgCl_3(H_2O)^{2-}$ (resembling $AgCl_4^{3-}$ in which one of the remote Cl is replaced by a water molecule) appears to be an intermediate complex between the "anhydrous" $AgCl_4^{3-}$ and $AgCl_2$. Anhydrous $AgCl_3^{2-}$ is a trigonal planar complex with a Ag-Cl average distance of 2.60 Å and Cl-Ag-Cl angles of 118°. Finally, $AgCl_2^-$ is a slightly bend complex with an average $R_{Ag\text{-}Cl}$ of 2.43 Å and a Cl-Ag-Cl angle of 168°. Note, however, the significant scatter in the Cl-Ag-Cl angular distribution, attaining ±10° at 1σ confidence level (Fig. 8b). The slightly different from linear Cl-Ag-Cl angles in the di-chloride complex revealed by MD are in better agreement with the EXAFS and XANES modeling above. Similar angles (~160°) were found for $AgCl_2^-$ by Liu et al. (2012) in their MD study. Deviations by 10-20° from a linear geometry were detected by XANES spectra modeling of the $Cu(I)Cl_2^-$ species in saline solutions similar to those of the study (Brugger et al., 2007).

Note that our optimizations of the $AgCl_2^-$ cluster in vacuum (i.e., without water molecules) revealed a linear Cl-Ag-Cl angle (179±1°) both at 0 and 300 K. This finding is also in line with static DFT quantum-chemistry calculations both in vacuum or using polarized continuum models for $AuCl_2^-$ (Pokrovski et al., 2009b) and $CuCl_2^-$ (Zajacz et al., 2011) that predict linear geometries (180±2°) for these species. However, optimizations of the full system ($AgCl_2^-$ with water molecules) systematically show a non-linear (168°) geometry of $AgCl_2^-$, even at 0 K, clearly demonstrating that this is a result of interactions of the $AgCl_2^-$ cluster with surrounding water molecules.

The angular structure of $AgCl_2^-$ revealed by MD simulations yields a non-zero dipole moment (~1.87 debye) for this species, as calculated from maximally localized Wannier orbitals (Marzari et al., 2012) for 30 snapshots extracted from the trajectory. This dipole value, comparable to that of an isolated water molecule (Silvestrelli and Parrinello, 1999) may be responsible for the stronger interactions of $AgCl_2^-$ than its Cu and Au analogs with surrounding water molecules. However, quantitative assessment of the strength of solute-water interactions for Cu, Ag, and Au would require more systematic comparative studies of these metals using similar modeling approaches.

As the temperature increases from 50 to 380°C, the average $R_{Ag\text{-}Cl}$ in $AgCl_2^-$ increases from 2.43 to 2.45 Å, while the Cl-Ag-Cl average angle decreases from 168 to 159°. For all the trajectories obtained at 380°C, $AgCl_2^-$ is found to be the most stable species. Simulations using either $AgCl_3^{2-}$ or $AgCl_4^{3-}$ as starting clusters showed their rapid (in less than 1 ps) dissociation to $AgCl_2^-$ plus one or two hydrated chlorine atoms. For the least concentrated Cl solution, the neutral $AgCl(H_2O)$ complex was also found as an intermediate species with a typical life-time of 15 ps for a total simulation time of 50 ps (Fig. EA4-2). In contrast with the absence of Na^+ ions at distances shorter than 6 Å at 50°C (see above), Na^+ was detected in the vicinity of $AgCl(H_2O)^0$, at distances between 3 and 4 Å from Ag (Fig. EA4-3).

In summary, the $AgCl_2^-$ complex is found at all conditions explored here, confirming the large stability of this species. This conclusion is in agreement with the recent theoretical MD study of Liu et al. (2012). However, in contrast to their study, we found persistence of the $AgCl_3^{2-}$ or $AgCl_4^{3-}$ complexes at moderate chlorine concentrations and low temperatures, in agreement with the present experimental XAS results. The stability of the $AgCl_4^{3-}$ complex is likely to have been overlooked by Liu et al. (2012) probably because of the smaller system size (48 water molecules) used in their study. It should be kept in mind that because of the finite duration of any FPMD simulation, an exhaustive determination of all possible species cannot be guaranteed. Quantifying the relative fractions of each species directly from the trajectories is beyond the reach of modern ab-initio MD simulations. Nonetheless, our simulations help to

test independently the stability of some selected species and to calculate their MD-EXAFS spectra, which may directly be compared with experimental data.

Typical MD-EXAFS spectra were generated for the complexes identified above using their corresponding subsets of trajectories. Fig. 9 compares the calculated MD-EXAFS spectrum of $AgCl_2^-$ at 380°C with the experimental spectrum at close conditions (exp#6, 400°C/750 bar, $m_{Cl^-} = 0.70$). The slight frequency shift between the two spectra visible in this figure is due to the known overestimation of the Ag-Cl nearest distances by typically 0.03 Å by FPMD calculations using the BLYP functional, as mentioned above (section 2.3). Except for this small difference, the very good agreement in shape, phase, and amplitude of the EXAFS signals between theory and experiment is both a robust validation of the numerical FPMD model and a confirmation of the predominance of $AgCl_2^-$ at these temperature and chlorine concentration.

The MD-EXAFS spectra shown in Fig. 10a illustrate the effect of temperature for $AgCl_2^-$. It can be seen that changes in the signal frequency between 50 and 380°C are very small, implying a weak effect of temperature on EXAFS spectra, which is mainly a result of slight variations in the Ag-Cl coordination shell (Fig. 8a). By contrast, more marked phase shifts are visible at a given temperature between the spectra of $AgCl_2^-$ and $AgCl_4^{3-}$ on one hand, and $AgCl_3^{2-}$ on the other (Fig. 10b). The phase shift of the $AgCl_3^{2-}$ spectrum to lower frequencies is due to longer Ag-Cl average distances in this complex (2.60 Å) compared to those in $AgCl_2^-$ (2.43 Å) and the two shortest distances in $AgCl_4^{3-}$ (2.47 Å). Note that the two longest Ag-Cl distances in the latter species (3.48 Å) have negligible contribution to EXAFS. The MD calculated phase shifts are in excellent agreement with experimental EXAFS spectra (Fig. 3) suggesting a growing contribution of $AgCl_3^{2-}$ with decreasing T and increasing m_{Cl}. In addition, the MD calculated Ag-Cl distances for the dichloride $AgCl_2^-$ (2.38 Å, when corrected to the typical shift of 2% of the R value, see section 2.3) are identical to those derived from EXAFS fits of the 0.7m Cl solution, confirming again the predominance of this species at elevated temperatures and moderate salt contents.

4. DISCUSSION

4.1. Structure and stability of Ag-Cl complexes in saline solutions

The complementary EXAFS, XANES, and FPMD analyses reported in this study put new important constraints on the stoichiometry and stability of silver chloride complexes at elevated temperatures. The number of Cl atoms derived from EXAFS, the shape of XANES spectra, and molecular dynamics simulations, all converge to the predominance of dichloride complexes with minor contributions of tri-chloride and/or tetra-chloride, at least between 300 and 450°C and chloride concentrations below 3m. The fractions of these higher-order chloride species in the total dissolved amount of Ag for each T-P-m_{Cl} point of our study may be independently estimated either from the experimental mean Ag-Cl coordination numbers or from Ag-Cl distances derived from EXAFS fits and coupled with the data on each individual species coordination number and distance from FPMD modeling (Table 2). In these calculations, we adopted Ag-Cl distances of 2.38±0.01 and 2.60±0.05 Å for $AgCl_2^-$ and $AgCl_3^{2-}$, respectively. Note that the percentage of the $AgCl_4^{3-}$ species cannot be evaluated using this approach because only the two nearest Cl atoms at ~2.4 Å in this species are unambiguously detected by EXAFS, whereas the two other Cl atoms at longer distances (~3.4 Å, Fig. 7) give negligible EXAFS signal. Consequently, the tetra-chloride species is almost identical in its EXAFS pattern to the di-chloride complex (e.g., Fig. 10). It can be seen in Table 2 that the fractions of $AgCl_3^{2-}$ in the total dissolved Ag derived from the N and R values are in agreement with one another within errors and do not exceed 20-30% in all experiments at T > 300°C. At 200 and 300°C, these fractions are somewhat higher for most concentrated salt solutions, up to ~50%, but the associated uncertainties do not allow more precise estimations.

These EXAFS-derived fractions of $AgCl_3^{2-}$ may also be compared with those calculated using thermodynamic properties of silver cation and its four chloride complexes reported in the literature. Note that according to all data sources, Ag^+, $AgCl^0$, and $AgOH^0$ fractions are less than 0.1% under our

experimental conditions, and thus dissolved silver is shared between $AgCl_2^-$ and $AgCl_3^{2-}$ ± $AgCl_4^{3-}$ (e.g., Fig. 1). Our tri-chloride species fractions are in marked disagreement with the speciation scheme of Sverjensky et al. (1997) that yields too large percentages of higher-order chloride species, $AgCl_3^{2-}$ and $AgCl_4^{3-}$, which are inconsistent with the EXAFS and FPMD results (Table 2). Similarly, the fractions of $AgCl_3^{2-}$ derived from the EXAFS parameters are systematically smaller at 200°C and 300°C in 2.6 and 5.9m Cl than those calculated using Seward's (1976) stability constants (40-70% $AgCl_3^{2-}$, Table 2). In contrast, the EXAFS-derived fractions are similar within errors in the whole temperature range to those calculated using the data for $AgCl_2^-$ from Akinfiev and Zotov (2001) and for $AgCl_3^-$ from Zotov et al. (1995). The above comparison thus suggests that $AgCl_2^-$ is likely to be the dominant species in the investigated T and m_{Cl} range, together with some contribution of $AgCl_3^{2-}$ whose fraction diminishes rapidly with increasing temperature and decreasing salinity.

Solubilities of $AgCl_{(s)}$ measured in situ from the absorption edge height of spectra at 200 and 300°C in this study (Table 1) provide an independent confirmation of these conclusions. It can be seen in Fig. 11 that the XAS-measured solubilities (Table 1) at 0.7 and 2.6m Cl are close to those predicted using the thermodynamic properties of $AgCl_2^-$ from Akinfiev and Zotov (2001) or Zotov et al. (1995) and assuming that it is the major species formed. Other data for $AgCl_2^-$ (not shown, Seward et al., 1976; Sverjensky et al., 1997) yield comparable (within errors) solubility values at such low-to-moderate Cl concentrations. At higher Cl (5.9m), the XAS solubilities are 2-3 times higher than those predictions, implying a contribution from higher-order Cl species. However, inclusion of $AgCl_3^{2-}$ from Seward (1976) or $AgCl_3^{2-}$ plus $AgCl_4^{3-}$ from Sverjensky et al. (1997) yields $AgCl_{(s)}$ solubilities at least 2 times higher than the XAS-measured values in the whole m_{Cl} range (Fig. 11). Thus, the stability of tri- and tetra-chloride complexes is likely to be overestimated at $T \leq 300$°C in those studies. At $T \geq 300$°C, the large stability of $AgCl_3^{2-}$ and $AgCl_4^{3-}$ predicted using Sverjensky et al.'s (1997) data is also incompatible with i) the EXAFS-derived Cl numbers of ~2.0±0.2 (Table 1), ii) the instability of $[AgCl_3]$ and $[AgCl_4]$ clusters revealed by molecular dynamics at 380°C (section 3.3), and iii) AgCl(s) solubility measured in situ in the 0.7m Cl solution at

300°C (0.049m , Table 1, versus 0.11-0.15m according to Sverjensky's or Seward's data). In contrast, our solubilities in the whole range of m_{Cl} at 200°C (Fig. 7) and in 0.7m Cl solutions at 300°C (Table 1) are in agreement, within better than 30% of the value, with thermodynamic predictions using $AgCl_2^-$ and $AgCl_3^{2-}$ properties from Akinfiev and Zotov (2001) and Zotov et al. (1995), respectively.

The fraction of the tetra-chloride species, detected by FPMD simulations at 50°C and 1.7m Cl, can be estimated neither from XAS data because of its spectral pattern very similar to that of $AgCl_2^-$ (see above), nor from published AgCl(s) solubility measurements because of the absence of reported stability constants for $AgCl_4^{3-}$ above 100°C in solutions of < 3m Cl (e.g., Seward et al., 1973). Nonetheless, two general criteria may be used to reject $AgCl_4^{3-}$ from the Ag speciation scheme at elevated temperatures and concentrated Cl solutions: a) the long Ag-Cl distances, 3.5 Å, for two of the four Cl atoms as found by FPMD at 50°C, are unlikely to persist at higher temperatures even in highly concentrated salt solutions because of the growing thermal disorder; b) the large negative charge of -3 of this complex will not be favored by the decreasing dielectric constant of the solution when T rises. Thus, $AgCl_4^{3-}$ is not stable and structurally defined enough to be considered as an individual silver complex at temperatures above 50-100°C. It may rather be regarded as $AgCl_2^-$ exhibiting outer-sphere interactions with free Cl^- and/or Na^+ ions in saline solutions. Note that the presence of Na^+ in the outer coordination sphere of Ag (R_{Ag-Na} > ~3 Å) is unlikely to be seen by XAS because of high thermal/structural disorder and loose Ag-Na bonds in such outer-sphere complexes, but it is detected by the MD-XAS calculations at m_{Cl} < 2m (see above). Thus, despite their relatively simple nearest-shell stoichiometry and geometry, the major silver complexes, $AgCl_2^-$ and $AgCl_3^{2-}$, are expected to exhibit significant interactions with the solvent and electrolyte in aqueous solution. This may account, at least partly, for the differences in the behavior of silver versus accompanying metals in hydrothermal fluids (section 4.3).

The discussion above allows for the following conclusions: 1) The majority of thermodynamic datasets for the dichloride species, $AgCl_2^-$ (Seward, 1973; Zotov et al., 1995; Sverjensky et al., 1997; Tagirov et al., 1997; Akinfiev and Zotov, 2001) are in fair agreement with one another as well as with the

dominant stoichiometry [Ag:Cl_2] inferred in this study at elevated T and low-to-moderate Cl contents. 2) The fraction of the tri-chloride species is likely to decrease fast with increasing T and decreasing salinity, in agreement with previous solubility data (Seward, 1976; Zotov et al., 1995). 3) The stability constants of $AgCl_3^{2-}$ and $AgCl_4^{3-}$ reported in the SUPCRT (Sverjensky et al., 1997) and other related databases (e.g., LLNL, Parkhurst and Appelo, 1999), which are all based on extrapolations from limited low-T data, are likely to be overestimated and should not be used above 100-200°C. 4) Based on the results of our study, we recommend the use of the stability constants of $AgCl_3^-$ from Zotov et al. (1995), to at least 300°C, and $AgCl_2^-$ from Akinfiev and Zotov (2001), at least in the T range 200-450°C. This dataset shows the best agreement with the XANES and EXAFS spectra and FPMD simulations of this work and AgCl(s) solubility of this and previous studies.

4.2. Comparison with other metals

The first experimental data for silver chloride complexes at hydrothermal conditions obtained in this study allow comparisons with Ag analogs, Cu and Au, and other metals common in geological fluids. The three metals, Cu, Ag, and Au, are monovalent in hydrothermal fluids and form predominantly single-charged di-chloride complexes at T above 250-300°C (e.g., Akinfiev and Zotov, 2001; Brugger et al., 2007; Pokrovski et al., 2008a, 2009b; this study). The formation of higher-order chloride species for Cu^I and Ag^I, $AgCl_3^{2-}$ (this study) and $CuCl_3^{2-}$ (Brugger et al., 2007), is limited to low and moderate temperatures (< 200-250°C) and high salt contents, and no tri- or tetra-chloride species have so far been reported for monovalent Au^I (Pokrovski et al., 2009b). SUPCRT-derived databases (e.g., Sverjensky et al., 1997; Parkhurst and Appelo, 1999) that use extrapolations from low-T data are likely to overestimate the amount of higher-order Cl complexes both for Cu (Brugger et al., 2007) and Ag (this study). The stability constants of the corresponding mono-, di- and tri-chloride complexes of Cu and Ag reported in recent studies (Akinfiev and Zotov, 2001; Brugger et al., 2007; as well as Sverjensky et al., 1997 for

mono- and di-chloride species) are similar within the data scatter, implying a similar affinity of both metals for the chloride ligand in aqueous solution over a wide T-range.

However, despite the large similarities in stoichiometry (amongst Cu, Ag, Au) and stability (between Cu and Ag) of chloride complexes, this study revealed some differences in the molecular structure of $AgCl_2^-$ compared to $CuCl_2^-$ and $AuCl_2^-$. The angular shape (∠Cl-Ag-Cl ~160°) and large Ag-Cl distances (R_{AgCl} ~2.38 Å) of the Ag complex contrast with the quasi-linear geometry and much shorter metal-Cl distances in its Au and Cu analogs, (∠Cl-Cu-Cl ~170-180°, R_{CuCl} ~2.12-2.15 Å, Fulton et al., 2000; Brugger et al., 2007; ∠Cl-Au-Cl ~180°, R_{AuCl} ~2.27 Å, Pokrovski et al., 2009b). The shortening of metal-chloride distances from Ag to Au may be partly explained by relativistic contraction of the Au^+ radius (Pyykkö, 1988). We are not aware of the existence of solid compounds in which Ag is two-coordinate by chlorides in a linear geometry; the available data show that Ag-Cl coordination geometries range from 3 to 6-coordinate. More generally, in contrast with Cu and Au, Ag rarely form two-coordinated complexes with other ligands in solids, preferring distorted penta-, tetra- or tri-coordinated geometries (ICSD, 2010). This tendency is also seen in aqueous solution, with the tetra-coordinated $Ag(H_2O)_4^+$ (this study) compared with the linear $Cu(H_2O)_2^+$ (Fulton et al., 2000). The higher Ag coordination than that of Cu and Au results in a pronounced maximum for the metal-oxygen distances in the row of the hydrated cations Cu^+-Ag^+-Au^+ ($R_{Cu\text{-}H2O}$ ~1.9 Å, Fulton et al., 2000; $R_{Ag\text{-}H2O}$ ~2.3 Å, Seward et al., 1996, this study; $R_{Au\text{-}H2O}$ ~2.0 Å, Feller et al., 1999). The tendency of Ag to form higher coordinated and less compact complexes than Cu and Au is also expressed in the angular shape and large Ag-Cl distances in $AgCl_2^-$ offering a less screened environment for Ag^+ and favoring outer-sphere interactions with ions and solvent molecules in the fluid, compared to the more compact linear $CuCl_2^-$ and $AuCl_2^-$. These structural differences may partly be responsible for the fractionation of Ag vs Cu and Au in brine-vapor-melt systems (section 5.1 below).

The molecular environment of metals such as Zn, Cd, Co, and Fe in saline hydrothermal solutions appears to be different. Although all these divalent metals are also transported as chloride complexes in

the great majority of crustal fluids (Wood and Samson, 1998; Yardley, 2005; Pokrovski et al., 2008a; Bazarkina et al., 2010), they form octahedral or tetrahedral entities containing both chloride and water in the first coordination sphere of the metal cation, as shown by UV-visible and XAS measurements (Susak and Crerar, 1985; Bazarkina et al., 2010; references therein). The octahedral-to-tetrahedral transition in the metal coordination takes place with increasing both the temperature and the number of Cl ligands in the dominant complex, so that low-order chloride species are octahedral (e.g., $Zn(H_2O)_5Cl^+$, $Fe(H_2O)_5Cl^+$, $Cd(H_2O)_5Cl^+$) and high-order tetrahedral (e.g., $ZnCl_4^{2-}$, $FeCl_4^{2-}$, $CdCl_3H_2O^-$). This may be explained qualitatively by partial charge constraints on the Cl and H_2O ligands when increasing the number of Cl atoms in the complex (Jolivet et al., 1994), and by the growth of thermal disorder with T favoring more compact (and thus less coordinate) species of lower entropy (Brimhall and Crerar, 1987). However, the major discrepancies in this picture concern the di-chloride complexes of these metals, in particular Zn and Fe, which were believed to be dominant in high T geological fluids of low dielectric constant that favors the stability of uncharged and weakly charged species (e.g., Brimhall and Crerar, 1987). First, it remains unclear whether such di-chloride complexes are tetrahedral or octahedral (i.e., the only difference is by two water molecules in the first shell of the metal) and whether they may exist in both coordinations. Second, there exist large discrepancies between mineral solubility data, which systematically indicate the dominant formation of di-chloride complexes in moderate-to-high saline fluids ($m_{Cl} > 0.1$m) at T > 250-300°C for both zinc and iron(II) (Ruaya and Seward, 1986; Bourcier and Barnes, 1987; Cygan et al., 1994; Fein et al., 1992; Ohmoto et al., 1994; Yardley, 2005), and recent XAS measurements in Fe and Zn chloride solutions, which report the predominance of double-charged tetra-chloride complexes, $FeCl_4^{2-}$ and $ZnCl_4^{2-}$, at similar conditions (e.g., Mayanovic et al., 1999; Testemale et al., 2009). Resolving these discrepancies requires combined studies using new molecular modeling approaches (e.g., MD and XANES modeling) and in situ spectroscopy, potentiometry, and solubility techniques. The impact of these discrepancies on the interpretation of metal transport and deposition by geological fluids remains to be understood.

5. IMPLICATIONS FOR Cu-Ag-Au FRACTIONATION IN HYDROTHERMAL PROCESSES

5.1. Structural control: vapor-brine and fluid-melt partitioning

The results of this study, together with the recent published work on Au and Cu aqueous speciation and solubility, help to appreciate the impact of structural differences among dissolved metal species on the behavior of Ag, Cu, and Au in natural hydrothermal-magmatic systems. These differences primarily affect the partitioning of the metals between brine, melt, and vapor phases. The angular structure of the Ag di-chloride complex, yielding a non-zero dipole moment likely favoring stronger interactions with outer sphere Na, Cl, and H_2O as compared to its Cu and Au analogs, may account for the elevated affinity of Ag for the hydrothermal brine phase. It explains the stronger partitioning of Ag than Cu or Au in favor of the brine in vapor-brine and melt-brine systems as observed in natural fluid inclusions from hydrothermal-magmatic deposits and laboratory experiments. For example vapor/brine and melt/brine partition coefficients of Ag ($K = C_{vapor}/C_{brine}$, or C_{melt}/C_{brine}, where C is Ag concentration in the corresponding phase) in water-salt sulfur-free laboratory systems at hydrothermal-magmatic conditions are up a factor of 10 lower than those of Cu (Pokrovski et al., 2005a; Simon et al., 2006, 2008). Natural data from coexisting low-to-moderate salinity fluid (< 1-3 m_{Cl}) and silicate melt inclusions from granitic systems display similar differences ($K_{fluid/melt}$ ~1-10 and ~10-1,000 for Ag and Cu, respectively, Zajacz et al., 2008), which confirms the weaker Ag versus Cu affinity for the low saline fluid phase. By contrast, Ag and Cu partitioning is similar between highly saline fluid and silicate melt inferred from the same type of inclusions ($K_{fluid/melt}$ ~10-50 for both Ag and Cu). In addition, $K_{fluid/melt}$ values of Ag systematically increase in favor of the fluid with increasing chloride content, whereas those of Cu show no clear correlation with m_{Cl} (Zajacz et al., 2008). Similar elevated Ag partition coefficients between 30 wt% salt brine and silicate melt ($K_{fluid/melt}$ ~ 50), comparable to those for Zn and Pb, were recently reported in granitic pegmatites (Borisova et al., 2012).

5.2. Chemical speciation control: chloride versus sulfide

The differences in metal partitioning are further accentuated by the presence of reduced sulfur that further increases Cu (and Au) volatility compared with Ag. For example, vapor/brine partitioning coefficients ($K_{vapor/brine}$) of metals in S-rich (up to 1-2 wt% H_2S+SO_2 in the vapor phase) porphyry systems (e.g., Seo et al., 2009; Kouzmanov and Pokrovski, 2013; references therein) and laboratory experiments (Pokrovski et al., 2008a) increase in the order Fe ≈ Zn < Ag < Cu < Au, attaining values of ~50 in favor of the vapor phase for Au due to the formation of volatile complexes with sulfur (H_2S and/or SO_2). The lowest volatility of base metals (typical $K_{vapor/brine}$ for Fe and Zn ~ 0.001-0.1, Kouzmanov and Pokrovski, 2012) is a direct consequence of i) their weak affinity for reduced sulfur ligands (Wood and Samson, 1998) and ii) the large stability of their hydrated chloride complexes in the high-salinity aqueous solution (section 4.2). Both elevated absolute copper concentrations in some natural vapor-like inclusions from porphyry deposits (~1000 ppm) and the corresponding $K_{vapor/brine}$ values above 1 should now be regarded as post-entrapment modifications due to preferential diffusion of Cu from the external fluid into the S-rich inclusion as suggested by recent experiments (Lerchbaumer and Audetat, 2012), whereas Au and Ag are unlikely to be affected by this phenomenon. Thus, the majority of experimental studies show Cu vapor-brine partition coefficients to be between those of Ag and Au (see Kouzmanov and Pokrovski, 2013 for a recent review). The highest volatility of Au in the order above is consistent with the far larger stability of its known sulfide complexes compared to other metals and, in particular, the formation of neutral and weakly polar species with hydrogen sulfide (e.g., $Au(H_2S)HS^0$, Pokrovski et al., 2009a), which are expected to be stable in the vapor phase of low density and dielectric constant. In contrast, the higher volatility of Cu than Ag in such S-rich systems is not consistent with the very similar stabilities and stoichiometries of their chloride and sulfide complexes in dense aqueous solution (see section 4.2). It may thus be hypothesized that structural differences exist between Ag and Cu species in both the low-density H_2S-rich vapor and saline liquid phase, which are fundamentally related to the tendency of Ag to form

larger and higher-coordinated complexes than Cu. Thus, the contrasting affinity for chloride versus sulfide ligands of Ag, Au, and base metals, together with structural differences amongst complexes of the same ligand type, account for the volatility trends. These trends may explain the enrichment by Au and partly Cu, compared to Ag and base metals, of certain types of epithermal ore deposits regarded as being formed by ascending magmatic vapor (e.g., high sulfidation Cu-Au, Heinrich et al., 1999; Carlin-type Au deposits, Muntean et al., 2011; refs therein).

5.3. Solid-phase control: mineral solubility

If the structure and stability of dissolved metal complexes are the primary factors controlling the metal fractionation in fluid/melt and vapor/brine systems, in the presence of solid phases, another fundamental factor affecting the metal behavior during the formation of hydrothermal deposits is the identity and stability of the major metal-bearing minerals themselves. They are, respectively, chalcopyrite ($CuFeS_2$), argentite/acanthite (Ag_2S), and native gold (Au) for Cu, Ag, and Au in the great majority of deposits. Although Ag also forms complex sulfosalts with As, Sb and Cu, their solubility trends can be reasonably approximated by the Ag_2S component. In low-temperature deposits, silver and gold may also form alloys with Au contents as low as 40%, but this has a minor affect on Au solubility trends by lowering Au activity in the solid and solution by only a factor of 2 to 3, which is insignificant compared to the variations of several orders of magnitude in Au concentrations in natural hydrothermal fluids (Kouzmanov and Pokrovski, 2012). Thus $CuFeS_2$, Ag_2S, and Au may be used as model compounds for identifying the major trends in the behavior of these metals during fluid-rock interactions. Below we briefly summarize the main differences in the solubility patterns of these metals in hydrothermal systems.

The solubility controlling reactions for these metals in the majority of hydrothermal contexts are the following:

$$AgCl_2^- + 0.5\ H_2S = 0.5\ Ag_2S(s) + H^+ + 2Cl^- \quad (1)$$

$$Au(HS)_2^- + 0.5H_2 + H^+ = Au(s) + H_2S, \text{ in near-neutral and alkaline fluids} \quad (2a)$$

$$AuHS^0 + 0.5H_2 = Au(s) + H_2S, \text{ in acidic fluids} \quad (2b)$$

$Au(HS)H_2S^0 + 0.5H_2 = Au(s) + 2H_2S$, in acidic S-rich fluids and possibly vapors (2c)

$AuCl_2^- + 0.5H_2 = Au(s) + H^+ + 2Cl^-$, above 500°C in acidic saline fluids (2d)

$CuCl_2^- + FeCl_2^0 + 2H_2S = CuFeS_2(s) + 3H^+ + 0.5\ H_2 + 4\ Cl^-$ (3a)

$CuCl_2^- + FeS_2(s) + 0.5H_2 = CuFeS_2(s) + H^+ + 2Cl^-$ (3b)

The differences in the major aqueous species and solid phases among these metals yield fundamentally different solubility trends versus pH, H_2S and salinity for Ag and Cu on one side and Au on the other. Fig. 12 shows the solubility of all three minerals as a function of pH, H_2S and Cl in a typical hydrothermal fluid at 400°C and 0.5 kbar (i.e., conditions in the middle of the T-P range of their deposits formation), and as a function of temperature at 0.3-1.0 kbar, calculated using the stability constants available for these reactions from sources indicated in the figure caption. It can be seen that at a given T-P, the factors leading to the deposition of Au vs Ag and Cu are opposite. Gold precipitation requires: a) removing reduced sulfur from the fluid (e.g., via reaction with Fe-rich rocks, fluid boiling); b) acidifying the near-neutral fluid (e.g., SO_2 disproportionation into sulfuric acid and H_2S, common in porphyry systems); c) reducing the fluid (e.g., reaction with organic-rich sediments). In contrast, both Ag and Cu precipitation requires: a) removing chloride (e.g., dilution with meteoric waters), b) neutralizing the fluid (e.g., reaction with carbonate rocks, which is typical of skarns), c) oxidizing the fluid (e.g., mixing with meteoric waters, reaction with ferric-iron sediments). Note that addition of reduced sulfur into the system (e.g., via disproportionation of SO_2 into sulfide and sulfate in a cooling magmatic fluid or reaction with S-rich sedimentary rocks) decreases the solubility of silver in contrast to Au (Fig. 12d), but has no effect on the solubility of the $CuFeS_2$-FeS_2 assemblage (H_2S is not involved in reaction 3b). In addition, some of the factors listed above may operate in an opposite way (e.g., dilution with meteoric oxidizing waters will lower both Cl and H_2S concentrations, which have an opposite effect on the solubility of Ag and Cu-bearing sulfides, see reactions 1 and 3a,b), so that the final result on the mineral solubility will be an interplay between all these factors in a given natural case. The only common effect on all three elements is temperature whose decrease leads to a drop in solubility but of different amplitude depending of the metal (Fig. 12a).

The major differences in Au vs Ag solubility apparent in Fig. 12 account, at least partly, for the Au/Ag ratios found in different types of deposits. For example, elevated Au/Ag ratios (typically 1-100) and high Au fineness (i.e., Au fraction in Ag-Ag alloys) generally occur in Au-Te, Cu-Au epithermal, skarn and gold orogenic deposits characterized by neutral-to-alkaline low-to-moderately saline fluids (e.g., Morrison et al., 1991; Pal'yanova, 2008) having a high capacity to concentrate and transport gold (Fig. 12b). Carlin-type Au and some Cu-Au high-sulfidation deposits are also characterized by elevated Au/Ag ratios consistent with their likely formation by S-rich magmatic vapor phases carrying preferentially Au as sulfide complexes (Pokrovski et al., 2008a; Muntean et al., 2011; references therein). Lower Au/Ag ratios (~0.001-10) are typical for epithermal alunite and adularia Au-Ag deposits (Sillitoe and Hedenquist, 2003; Pal'yanova, 2008; references therein) formed by acidic fluids of elevated salinity (10-20 wt% NaCl) favorable for Ag solubility (see Fig. 12b,c).

Although it is more difficult to place Cu in this picture of solubility control because of its much greater abundance than Ag and Au in most types of fluids, some qualitative trends in Cu vs Ag and Au fractionation may still be identified in certain types of ore deposits. For example, despite large variations of Cu/Au ratios in porphyry-style Cu-Au-Mo deposits (from 10^3 to 10^6), they roughly increase with depth (Murakami et al., 2010). This was qualitatively interpreted by the more efficient precipitation of chalcopyrite than gold from an ascending cooling magmatic fluid carrying Cu in the form of chloride complexes, whereas Au remained in the fluid as soluble sulfide species (Murakami et al., 2010). Fig. 12a shows $CuFeS_2$, Ag_2S and Au solubility in a 10wt% salt fluid as a function of temperature at pressure progressively decreasing from 1000 bar at 550°C to 300 bar below 300°C under redox and acidity conditions buffered by silicate and Fe sulfide and oxide mineral assemblages typical of porphyry-style deposits (e.g., Sillitoe, 2010; references therein). It can be seen that the slope of the $CuFeS_2$ solubility curve is indeed significantly steeper than that of Au in the T range 300-500°C, in which major ore deposition occurs in porphyry deposits. This temperature dependence of solubility, coupled with the 1,000 times higher amount of Cu compared to that of Au in the fluid, leads to massive Cu precipitation with

temperature drop. The solubility of Ag_2S at such conditions is comparable with that of $CuFeS_2$, with concentrations of 100's ppm Ag (Fig. 12). This is, however, typically 10 to 50 times higher than typical abundances of Ag in natural moderate-salinity fluids and melts as inferred from inclusions (Kouzmanov and Pokrovski, 2012; references therein). Most of saline high-T fluids are thus under-saturated with respect of Ag-bearing solid phases. This explains the rarity of hydrothermal silver minerals at T > 300-350°C, and the fact that most silver resources are found in low-temperature epithermal deposits formed below 300°C. This distinguishes Ag from Au and Cu that form hydrothermal deposits in a wide T range from ~600 down to 150°C, and is thus a direct consequence of the solubility of their major minerals.

As a conclusion, the structure and stoichiometry of chloride complexes of Ag and accompanying metals should be taken into account when interpreting metal fractionations in fluid-vapor and fluid-melt systems. It seems to exert a lesser effect, however, on the metal behavior in mineral-fluid systems where differences in the nature of the ligand in the dominant dissolved complexes (chloride for Ag, chloride and possibly sulfide for Cu, and sulfide for Au), coupled with differences in the chemistry and solubility of their principal minerals (sulfides for Cu and Ag, native metal for Au), largely control the metal transport by crustal fluids and vapors and their precipitation as hydrothermal ores.

6. CONCLUDING REMARKS

This report is the first measurement, to the best of our knowledge, that uses in situ X-ray absorption spectroscopy to determine the stability and structure of Ag(I) chloride-bearing complexes in aqueous fluids pertinent to hydrothermal-magmatic systems. The combination of XANES and EXAFS spectra analyses, molecular dynamics modeling of structures of Ag-Cl aqueous complexes, and in situ solubility measurements of our study with thermodynamic analysis of published datasets provide new constraints on the identity, structure, and stability of major Ag-Cl species operating in natural hydrothermal fluids. The following major conclusions have been reached.

1) The silver di- and tri-chloride complexes, $AgCl_2^-$ and $AgCl_3^{2-}$, are the major species forming in moderate-temperature (200-300°C) aqueous solutions in a wide range of salinity (to at least 6m Cl, corresponding to ~26 wt% NaCl equivalent). These species have an angular and triangular geometry, respectively, with mean Ag-Cl distances of ~2.40 ($AgCl_2^-$) and 2.55 Å ($AgCl_3^{2-}$). The non-linear geometry of $AgCl_2^-$ revealed by MD and XANES modeling (angle Cl-Ag-Cl ~ 160°) is due to interactions with surrounding water molecules and increasing dynamic disorder with temperature in aqueous solution. The fraction of the tri-chloride species decreases with increasing temperature and decreasing chloride concentration, so that $AgCl_2^-$ becomes by far the major Ag-transporting complex at elevated temperatures (> 350°C) in typical magmatic-hydrothermal fluids. Both species exhibit long-range interactions with the surrounding water molecules and salt ions as revealed by MD simulations. The tetra-chloride complex, $AgCl_4^{3-}$, suggested in previous work at low-temperatures (< 150°C), may be regarded as $AgCl_2^-$ exhibiting outer-sphere electrostatic interactions with two from four Cl^- ligands at distances > 3 Å. The coordination environment of Ag in its dominant species in solution appears to be different from that of most Ag-bearing solids, in which Ag has distorted coordination geometries with 3 to 6 Cl/O atoms, and from Cl-free acidic solutions, in which the Ag^+ cation forms a distorted hydration sphere with 4 to 6 H_2O molecules.

2) The species fractions derived from XAS and MD analyses, together with XAS-measured AgCl(s) solubility, are in excellent agreement with thermodynamic predictions using the stability constants of $AgCl_2^-$ and $AgCl_3^{2-}$ from Akinfiev and Zotov (2001) and Zotov et al. (1995), respectively, that are based on extensive AgCl(s) solubility experiments. Our data also qualitatively agree with the pioneering AgCl(s) solubility measurements of Seward (1976). In contrast, our results disagree with SUPCRT-based datasets for Ag-Cl species (e.g., Sverjensky et al., 1997; Parkhurst and Angelo, 1999) derived by extrapolation from low-temperature data, which predict large fractions of the high-order chloride species, $AgCl_3^{2-}$ and $AgCl_4^{3-}$, in high-temperature fluids. Thus, we recommend the thermodynamic set of Zotov's

group for chemical equilibrium calculations in Ag-bearing mineral-fluid systems above 200°C. A full set of revised HKF parameters for silver chloride complexes will be presented in a future contribution.

3) Silver chloride complexes found in this work have longer Ag-Cl distances and stronger outer-sphere interactions with the solvent and electrolytes than their Au and Cu counterparts. This may explain the preferential partitioning of Ag into brine in brine-vapor and brine-melt magmatic-hydrothermal systems compared with Cu and Au, as observed in natural melt and fluid inclusions and laboratory experiments.

4) However, details of molecular structure of Ag, Cu, and Au complexes (geometry, inter-atomic distances and solute-solvent interactions) matter much less in sulfur-rich hydrothermal environments and most fluid-mineral systems where the contrasting affinity of these metals for sulfur ligands (with Au forming far more stable complexes than Ag and Cu with reduced sulfur), coupled with the different stability of their main solid phases (Ag sulfides, Cu-Fe sulfides, and native Au), largely controls the transport and distribution of these metals by geological fluids and Ag/Au/Cu ratios in economic deposits.

Acknowledgements: This work was supported by CNRS grants from the French GDR Transmet, 3F (Fluides-Failles-Flux), INSU-Actions Innovantes (CO2MET) programs, funds from the Laboratoire Européen Associé Géochimie Environnementale (LEAGE), and the Agence Nationale de la Recherche (grant SOUMET - ANR 2011 Blanc SIMI 5-6 009), and by granted access to the HPC resources of CINES/IDRIS under the allocation 2011-082309 from GENCI (Grand Equipement National de Calcul Intensif). We are grateful to the ESRF committee for providing beam time and access to the synchrotron facility, G. Ciatto for his assistance at BM29 beamline, and D. Testemale and Y. Joly for their help with XANES spectra modeling. Tatiana Pokrovski is acknowledged for her assistance in the manuscript revision. Thoughtful reviews of T. Kashiwabara and two anonymous referees greatly improved this article.

References

Akinfiev, N.N., Zotov, A.V., 1999. Thermodynamic description of equilibria in mixed fluids (H_2O-non-polar gas) over a wide range of temperature (25-700°C) and pressure (1-5000 bars). Geochim. Cosmochim. Acta **63**, 2025-2041.

Akinfiev N.N. and Zotov A.V. (2001) Thermodynamic description of chloride, hydrosulphide, and hydroxide complexes of Ag(I), Cu(I), and Au(I) at temperatures of 25-500°C and pressures of 1-2000 bar. Geochem. Intern. **39** (10), 990-1006.

Akinfiev N.N., Baranova N.N., Zotov A.V. and Tagirov B.R. (2008) Thermodynamic description of aqueous components in the system Cu-Ag-Au-S-Se-O-H in the range of temperatures 0-600°C and pressures 1-3000 bars. In Experimental studies of endogenic processes (eds. I. D. Ryabchikov, Yu. B. Shapovalov, E. G. Osadchii). Publishing Office of the Institute of the Problems of Chemical Physics, Chernogolovka, Russia, pp. 184-203 (in Russian).

Armunanto R., Schwenk C.F., Rode B.M. (2003) Structure and dynamics of hydrated Ag(I): Ab initio quantum mechanical-molecular mechanical molecular dynamics simulation. J. Phys. Chem. A, **107**, 3132-3138.

Anderko A. and Pitzer K.S. (1993) Equation-of-state representation of phase-equilibria and volumetric properties of the system NaCl-H_2O above 573 K. Geochim. Cosmochim. Acta **57**, 1657-1680.

Audédat A., Günther D., and Heinrich C.A. (2000) Causes for large-scale metal zonation around mineralized plutons: Fluid inclusion LA-ICP-MS evidence from the Mole Granite, Australia. Econ. Geol. **95**, 1563-1581.

Bakker R.J. (2003) Package FLUIDS 1. Computer programs for analysis of fluid inclusion data and for modelling bulk fluid properties. Chem. Geol. **194**, 3-23.

Bazarkina E.F., Pokrovski G.S., Zotov A.V., Hazemann J-L. (2010) Structure and stability of cadmium chloride complexes in hydrothermal fluids. Chem. Geol. **276**, 1-17.

Becke A. (1988) Density-functional exchange-energy approximation with correct asymptotic behavior. Phys. Rev.A **38,** 3098–3100.

Bernasconi L., Blumberger J., Sprik M., Vuilleumier R. (2004) Density functional calculation of the electronic absorption spectrum of Cu^+ and Ag^+ aqua ions. J. Chem. Phys. **121**, 11885-11899.

Berry A.J., Harris A.C., Kamenetsky V.S., Newville M., Sutton S.R. (2009) The speciation of copper in natural fluid inclusions at temperatures up to 700°C. Chem. Geol. **259**, 1-6.

Borisova A.Y., Thomas R., Salvi S., Candaudap F., Lanzanova A., Chmeleff J. (2012) Tin and associated metal and metalloid geochemistry by femtosecond LA-ICP-QMS microanalysis of pegmatite-leucogranite melt and fluid inclusions: new evidence from melt-melt-fluid immiscibility. Miner. Mag. **76**, 91-133.

Bourcier W. L., Barnes H. L. (1987) Ore solution chemistry-VII. Stabilities of chloride and bisulfide complexes of zinc to 350°C. Econ. Geol. **82**, 1839–1863.

Brimhall G.H. and Crerar D.A. (1987) Ore fluids: magmatic to supergene. Rev. Miner. **17**, 235-321.

Brugger J., Etschmann B., Liu W., Testemale D., Hazemann J.L., Emerich H., Van Beek W., Proux O. (2007). An XAS study of the structure and thermodynamics of Cu(I) chloride complexes in brines up to high temperature (400°C, 600 bar). Geochim. Cosmochim. Acta **71**, 4920-4941.

Crerar D., Wood S. and Brantley S. (1985) Chemical controls on solubility of ore-forming minerals in hydrothermal solutions. Can. Miner. **23**, 333-352.

Cygan G. L., Hemley J. J., D'Angelo W. M. (1994). An experimental study of zinc chloride speciation from 300 to 600°C and 0.5–2.0 kbar in buffered hydrothermal solutions. Geochim. Cosmochim. Acta **58**, 4841–4855.

Dang L.X., Schenter G.K., Glezakou V.A. and Fulton J.L. (2006) Molecular simulation analysis and X-ray absorption measurement of Ca^{2+}, K^+ and Cl^- ions in solution, J. Phys. Chem. B **110**, 23644-23654.

D'Angelo P., Migliorati V., Mancini G. and Chellemi G. (2008) A coupled molecular dynamics and XANES data analysis investigation of aqueous cadmium(II). J. Phys. Chem. A **112**, 11833-11841.

Etschmann B.E., Liu W., Testemale D., Müller H., Rae N.A., Proux O., Hazemann J.L., Brugger J. (2010) An in situ XAS study of copper(I) transport as hydrosulfide complexes in hydrothermal solutions (25-592°C, 180-600 bar): Speciation and solubility in vapor and liquid phases. Geochim. Cosmochim. Acta **74**, 4723-4739.

Fein J.B., Hemley J.J., d'Angelo W.M., Komninou A., Sverjensky D.A. (1992) Experimental study of iron-chloride complexing in hydrothremal fluids. Geochim. Cosmochim. Acta **56**, 3179-3190.

Feller D., Glendening E. D. and Jong, W. A. (1999) Structures and binding enthalpies of $M^+(H_2O)_n$ clusters, M=Cu, Ag, Au. J. Chem. Phys. **110**, 1475-1491.

Ferlat G., San Miguel A., Jal J. F., Soetens J. C., Bopp Ph. A., Hazemann J. L., Testemale T., Daniel I. (2002) The quest for ion pairing in supercritical aqueous electrolytes. J. Mol. Liq. **101**, 127-136.

Ferlat G., Soetens J. C., San Miguel A., Bopp Ph. A. (2005) Combining extended x-ray absorption fine structure with numerical simulations for disordered systems. J. Phys. Condens. Matter **17**, S145-S157.

Filipponi A., Borowski M., Bowron D.T., Ansell S., De Panfilis S., Di Cicco A., Itie J.-P. (2000) An experimental station for advanced research on condensed matter under extreme conditions at the European synchrotron radiation facility - BM29 beamline. Rev. Sci. Instruments **71**, 2422-2432.

Fulton J.L., Hoffmann M.M., Darab J.G. (2000) An X-ray absorption fine structure study of copper(I) chloride coordination structure in water up to 325°C. Chem. Phys. Lett. **330**, 300-308.

Fulton J.L., Kathmann S.M., Schenter G.K., Balasubramanian M. (2009) Hydrated structure of Ag(I) ion from symmetry-dependent, K- and L-edge XAFS multiple scattering and moleculer dynamics simulations. J. Phys. Chem A **113**, 13976-13984.

Gammons C.H. (1995) Experimental investigations of hydrothremal geochemistry of Pt and Pd. IV. The stoichiometry of Pt(IV) and Pd(II) chloride complexes at 100 to 300°C. Geochim. Cosmochim. Acta **59**, 1655-1668.

Gammons C.H., Williams-Jones A.E. (1995) The solubility of Au-Ag alloy + AgCl in HCl/NaCl solutions at 300°C: New data on the stability of Au(I) chloride complexes in hydrothermal fluids. Geochim. Cosmochim. Acta **59**, 3453-3468.

Gammons C.H. and Seward T.M. (1996) Stability of manganese(II) chloride complexes from 25 to 300°C. Geochim. Cosmochim. Acta **60**, 4295-4311.

Gammons C.H., Yu Y. (2007) The stability of aqueous silver bromide and iodide complexes at 25–300°C: Experiments, theory and geologic applications. Chem. Geol. **137**, 155-173.

Gammons C.H., Wood S.A., Williams-Jones A.E. (1996) The aqueous geochemistry of rare earth elements and yttrium: VI. Stability of neodymium chloride complexes from 25 to 300°C. Geochim. Cosmochim. Acta **60**, 4615-4630.

Gibbons C.S., Trotter J. (1971) Crystal structure of exo-Tricyclo[3,2,1,$0^{2,4}$]oct-6-ene-silver nitrate, and a refinement of the silver nitrate structure. J. Chem. Soc. A, 2058-2062.

Godinho S.S.M.C., Cabral do Couto P., Costa Cabral B.J. (2005) Polarization effects and charge separation in AgCl-water clusters. J. Chem. Phys. **122**, 044316, 1-14.

Goedecker S., Teter M., and Hutter J. (1996). Separable dual-space gaussian pseudopotentials. Physical Review B **54,** 1703–1710.

Grimme S. (2006). Semiempirical GGA-type density functional constructed with a long-range dispersion correction. J. Comput. Chem. **27**, 1787.

Hartwigsen C., Goedecker S., and Hutter J. (1998). Relativistic separable dual-space gaussian pseudopotentials from H to Rn. Physical Review B **58,** 3641–3662.

Heinrich, C.A., Günther, D., Audédat, A., Ulrich, T., Frischknecht, R, 1999. Metal fractionation between magmatic brine and vapour, and the link between porphyry-style and epithermal Cu-Au deposits. Geology **27**, 755-758.

Hull S. , Keen D. A. (1999) Pressure-induced phase transitions in AgCl, AgBr, and AgI. Phys. Rev. **B 59,** 750-761.

ICSD (2010) Inorganic Crystal Structure Database, FIZ Karlshure, http://www.fiz-karlsruhe.de/icsd.html

Inui M., Takeda S., Shirakawa Y., Tamaki S., Waseda Y., Yamaguchi Y. (1991) Structural study of molten silver halides by neutron diffraction. J. Phys. Soc. Japan **60**, 3025-3031.

Johnson J.W., Oelkers E.H. and Helgeson H.C. (1992) SUPCRT92: A software package for calculating the standard molal thermodynamic properties of minerals, gases, aqueous species, and reactions from 1 to 5000 bar and 0 to 1000°C. Computers & Geosci. **18**, 899-947; http://geopig.asu.edu/index.html#.

Jolivet J-P., Henry M., Livage J. (1994) *De la Solution à l'Oxide*. InterEditions & CNRS Editions, 249p.

Joly Y. (2001) X-ray absorption near-edge structure calculations beyond the muffin tin approximation. Phys. Rev. **B 63**, 125120.

KawakitaY., Enosaki T., Takeda S., Maruyama K. (2007) Structural study of molten Ag halides and molten AgCl-AgI mixture. J. Non-Cryst. Solids **535**, 3035-3039.

Kelly S.D., Hesterberg D., Ravel B. (2008) Analysis of soils and minerals using X-ray absorption specroscopy. Methods of Soil Analysis. Part 5. Mineralogical Methods, p. 387-463, Soil Sci. Soc. Am., Madison, USA.

Kouzmanov K., Pokrovski G.S. (2013) Hydrothermal controls on metal distribution in porphyry systems. Society of Economic Geologists Special Publication, accepted.

Krack M. (2005). Pseudopotentials for H to Kr optimized for gradient-corrected exchange- correlation functionals. Theor. Chem. Acc. **114,** 145-152.

Lee C., Yang W., and Parr R. (1988). Development of the colle-salvetti correlation-energy formula into a functional of the electron-density. Phys. Rev.B **37,** 785-789.

Lerchbaumer L., Audétat A. (2012) High Cu concentrations in vapor-type fluid inclusions: An artifact? Geochim. Cosmochim. Acta **88**, 255-274.

Lippert G., Hutter J., and Parrinello M. (1997). A hybrid gaussian and plane wave density functional scheme. Molecular Physics **92,** 477-487.

Liu X., Lu X., Wang R., Zhou H. (2012). Silver speciation in chloride-containing hydrothermal solutions from first principles molecular dynamics simulations. Chem. Geol. **294-295**, 103-112.

Malinowski E.R. (1991) Factor Analysis in Chemistry. 2nd Edition, Wiley.

Martell A.E., Smith R.M., Motekaitis R.J. (2004) Critical: Critically Selected Stability Constants of Metal Complexes Database. Version 8.0, NIST., Texas A & M University.

Martinez J.M, Pappalardo R.R., Sanchez-Marcos E. (1997) Study of the Ag^+ hydration by means of a semicontinuum quantum-chemical solvation model. J. Phys. Chem. A, **101**, 4444-4448.

Marzari N., Mostofi A.A., Yates J.R., Souza I., Vanderbilt D. (2012) Maximally localized Wannier functions: Theory and applications. Rev. Mod. Phys. **84**, 1419-1475.

Mayanovic R.A., Anderson A.J., Bassett W.A., Chou I.-M. (1999). XAFS measurements on zinc chloride aqueous solutions from ambient to supercritical conditions using the diamond anvil cell. J. Synchrotron Rad. **6**, 195-197.

Munoz, M., Argoul, P., Farges F., 2003. Continuous cauchy wavelet transform analyses of EXAFS spectra: a qualitative approach. Amer. Mineral. **88**, 694-700.

Mantean J.L., Cline J.S., Simon A.C., Longo A.A. (2011) Marmatic-hydrothremal origin of Navada's Carlin-type gold deposits. Nature Geoscience **4**, 122-127.

Morrison G.W., Rose W.J., Jaireth S. (1991) Geological and geochemical controls on the silver content (fineness) of gold-silver deposits. Ore Geol. Rev. **6**, 333-364.

Murakami H., Seo J.H., Heinrich C.A. (2010) The relation between Cu/Au ratio and formation depth of porphyry-style Cu-Au±Mo deposits. Miner. Deposita **45**, 11-21.

Newville M. (2001) IFEFFIT: interactive XAFS analysis and FEFF fitting. J. Synchrotron Rad. **8**, 322-324.

Nosé, S. (1984a). A molecular-dynamics method for simulations in the canonical ensemble. Mol. Phys. **52,** 255–268.

Nosé, S. (1984b). A unified formulation of the constant temperature molecular-dynamics methods. J. Chem. Phys. **81,** 511–519.

Ohmoto H., Hayashi K-I., Kajisa Y. (1994) Experimental study of the solubilities of pyrite in NaCl-bearing aqueous solutions at 250-350°C. Geochim. Cosmochim. Acta **58**, 2169-2185.

Pal'yanova G. (2008) Physicochemical modeling of the coupled behavior of gold and silver in hydrothremal processes: Gold fineness, Au/Ag ratios and their possible implications. Chem. Geol. **255**, 399-413.

Parkhurst, D.L., Appelo, C.A.J., 1999. User's guide to PHREEQC (version 2) - a computer program for speciation, reaction-path, 1D-transport, and inverse geochemical calculations. US Geol. Surv. Water Resour. Inv. Rep. 99-4259, 312p.

Persson I., Nilsson K.B. (2006) Coordination chemistry of the solvated silver(I) ion in thye oxygen donor solvents water, dimethyl sulfoxide, and N,N'-dimethylpropyleneurea. Inorg. Chem. **45**, 7428-7434.

Pokrovski G.S., Roux J. and Harrichoury J.-C. (2005a). Fluid density control on vapor-liquid partitioning of metals in hydrothermal systems. Geology **33**, 657-660.

Pokrovski G.S., Roux J., Hazemann J.-L. and Testemale D. (2005b) An X-ray absorption spectroscopy study of argutite solubility and germanium aqueous speciation in hydrothermal fluids to 500°C and 400 bar. Chem. Geol. **217**, 127-145.

Pokrovski G.S., Borisova A.Yu., Roux J., Hazemann J.-L., Petdang A., Tella M. and Testemale D. (2006). Antimony speciation in saline hydrothermal fluids: A combined X-ray absorption fine structure and solubility study. *Geochim. Cosmochim Acta* **70**, 4196-4214.

Pokrovski G.S., Borisova A.Yu. and Harrichoury J.-C. (2008a). The effect of sulfur on vapor-liquid fractionation of metals in hydrothermal systems. *Earth Planet. Sci. Lett.* **266**, 345-362.

Pokrovski G.S., Roux J., Hazemann J.-L., Borisova A.Yu., Gonchar A.A. and Lemeshko M.P. (2008b) In situ X-ray absorption spectroscopy measurement of vapor-brine fractionation of antimony at hydrothermal conditions. Min. Mag. **72**, 667-681.

Pokrovski G.S., Tagirov B.R., Schott J., Hazemann J.-L., Proux O. (2009a). A new view on gold speciation in sulfur-bearing hydrothermal fluids from in situ X-ray absorption spectroscopy and quantum-chemical modeling. Geochim. Cosmochim. Acta **73**, 5406-5427.

Pokrovski G.S., Tagirov B.R., Schott J., Bazarkina E.F., Hazemann J.-L. and Proux O. (2009b) An in situ X-ray absorption spectroscopy study of gold-chloride complexing in hydrothermal fluids. Chem. Geol. **259**, 17-29.

Pyykkö P. (1988) Relativistric effects in structural chemistry. Chem. Rev. **88**, 563-594.

Ravel B. and Newville M. (2005) ATHENA, ARTEMIS, HEPHAESTUS: data analysis for X-ray absorption spectroscopy using IFEFFIT. J. Synchrotron Rad. **12**, 537-541.

Robie R.A., Hemingway B.S. (1995) Thermodynamic Properties of Minerals and Related Substances at 298.15 K and 1 bar (10^5 pascals) pressure and at high temperatures. U. S. Geol. Surv. Bull. **2131**, 461p.

Rossberg A., Reich T., Bernhard G. (2003) Complexation of uranium(VI) with protocatechuic acid – application of iterative transformation factor analysis to EXAFS spectroscopy. Anal. Bioanal. Chem. **376**, 631-638.

Ruaya J.R. and Seward T.M. (1986) The stability of chloro-zinc (II) complexes in hydrothermal solutions up to 350°C. Geochim. Cosmochim. Acta **50**, 651-661.

Ruaya J.R. and Seward T.M. (1987) The ion-pair constant and other thermodynamic properties of HCl up to 350°C. Geochim. Cosmochim. Acta **51**, 121-130.

Rudnick, R.L., Gao, S., 2003. Composition of the Continental Crust. In: Holland, H.D., Turekian, K.K. (Eds.), Treatise on Geochemistry, Elsevier, Amsterdam.

Sandström M., Neilson G.W., Johansson G., Yamaguchi T. (1985) Ag^+ hydration in perchlorate solution. J. Phys. C: Solid State Phys. **18**, L1115-L1121.

Sayers D.E. (2000) Report of the International XAFS Society Standards and Criteria Commitee. http://www.i-x-s.org/OLD/subcommittee_reports/sc/.

Seward T.M. (1976) The stability of chloride complexes of silver in hydrothremal solutions up to 350°C. Geochim. Cosmochim. Acta 40, 1329-1341.

Seward T.M., Henderson C.M.B., Charnock J.M., Dobson B.R. (1996) An X-ray absorption (EXAFS) spectroscopic study of aquated Ag^+ in hydrothermal solutions to 350°C. Geochim. Cosmochim. Acta **60**, 2273-2282.

Sherman D.M. (2010) Metal complexation and ion association in hydrothermal fluids: insights from quantum chemistry and molecular dynamics. Geofluids **10**, 41-57.

Shvarov Y.S. (2008) HCh: New potentialities for the thermodynamic simulation of geochemical systems offered by windows. Geochem. Intl. **46**, 834-839; http://www.geol.msu.ru/deps/geochems/soft/index.html/

Skipper N.T., Neilson G.W. (1989) X-ray and neutron diffraction studies on concentrated aqueous solutions of sodium nitrate and silver nitrate. J. Phys.: Condens. Matter **1**, 4141-4154.

Sillitoe R.H. (2010) Porphyry copper systems. Econ. Geol. **105**, 3-41.

Sillitoe R.H., Hedenquist J.W (2003) Linkages between volcanotectonic settings, ore-fluid compositions, and epithermal precious metal deposits. Soc. Econ. Geol. Spec. Pub. **10**, 315-343.

Silvestrelli P.L., Parrinello M. (1999) Water molecule dipole in the gas and in the liquid phase. Phys. Rev. Lett. **82**, 3308-3311.

Simon A.C., Pettke T., Candela P.A., Piccoli P.M., Heinrich C.A. (2006) Copper partitioning in a melt–vapor–brine–magnetite–pyrrhotite assemblage. Geochim. Cosmochim. Acta **70**, 5583-5600.

Simon A.C., Pettke T., Candela P.A., Piccoli P.M. (2008) The partitioning behavior of silver in a vapor–brine–rhyolite melt assemblage. Geochim. Cosmochim. Acta **72,** 1638-1659.

Seo J.H., Guillong M., Heinrich C.A. (2009) The role of sulfur in the formation of magmatic-hydrothermal copper-gold deposits. Earth Planet. Sci. Lett. **282**, 323-328.

Sprik M., Hutter J., Parrinello M., (1996) Ab initio molecular dynamics simulation of liquid water: Comparison of three gradient-corrected density functionals. J. Chem. Phys. **105**, 1142-1152.

Stefánsson A., Seward T.M. (2003). Experimental determination of the stability and stoichiometry of sulphide complexes of silver(I) in hydrothermal solutions to 400°C. Geochim. Cosmochim. Acta **67**, 1395-1413.

Susak N.J., Crerar D.A. (1985) Spectra and coordination changes of transition metals in hydrothermal solutions: Implication for ore genesis. Geochim. Cosmochim. Acta **49**, 555-564.

Sverjensky D.A., Shock E.L. and Helgeson H.C. (1997) Prediction of the thermodynamic properties of aqueous metal complexes to 1000°C and 5 kb. Geochim. Cosmochim. Acta **61**, 1359-1412.

Tanger J.C., Helgeson H.C. (1988) Calculation of the thermodynamic and transport properties of aqueous species at high pressures and temperatures: Revised equations of state for the standard partial molal properties of ions and electrolytes. Amer. J. Sci. **288**, 19-98.

Tagirov, B.R., Zotov, A.V., Akinfiev, N.N., 1997. Experimental study of the dissociation of HCl from 350 to 500°C and from 500 to 2500 bar. Thermodynamic properties of HCl^0 (aq). Geochim. Cosmochim. Acta **61**, 4267-4280.

Testemale D., Hazemann J.-L., Pokrovski G.S., Joly Y., Roux J., Argoud R. and Geaymond O. (2004) Structural and electronic evolution of the $As(OH)_3$ molecule in high temperature aqueous solutions: An x-ray absorption investigation. J. Chem. Phys. **121,** 8973-8982.

Testemale D., Argoud R., Geaymond O. and Hazemann J.-L. (2005). High pressure/high temperature cell for x-ray absorption and scattering techniques. Rev. Sci. Instrum. **76**, 043905-043909.

Testemale D., Brugger J., Liu W., Etschmann B., Hazemann J-L. (2009) In-situ X-ray absorption study of iron(II) speciation in brines up to supercritical conditions. Chem. Geol. **264**, 295-310.

Texter J., Hastrelter J.J., Hall J.L. (1983) Spectroscopic confirmation of the tetrahedral geometry of $Ag(H_2O)_4^+$. J. Phys. Chem. **87**, 4690-4693.

Ulrich, T., Günther, D., Heinrich, C.A., 1999. Gold concentrations of magmatic brines and the metal budget of porphyry copper deposits. Nature **399**, 676-679.

VandeVondele J. and Hutter J. (2003). An efficient orbital transformation method for electronic structure calculations. J. Chem. Phys. **118,** 4365– 4369.

VandeVondele J., Krack M., Mohamed F., Parrinello M., Chassaing T., and Hutter J. (2005a). Quickstep: Fast and accurate density functional calculations using a mixed gaussian and plane waves approach. Comput. Phys. Comm. **167,** 103–128.

VandeVondele J., Mohamed F., Krack M., Hutter J., Sprik M., and Parrinello, M. (2005b). The influence of temperature and density functional models in ab initio molecular dynamics simulation of liquid water. J. Chem. Phys. **122**, 014515.

VandeVondele J. and Hutter J. (2007). Gaussian basis sets for accurate calculations on molecular systems in gas and condensed phases. J. Chem. Phys. **127,** 114105.

Webster J.G. (1986) The solubility of gold and silver in the system Au-Ag-S-O_2-H_2O at 25°C and 1 atm. Geochim. Cosmochim. Acta **50**, 1837-1845.

Williams-Jones A.E. and Seward T.M (1989) The stability of calcium chloride ion pairs in aqueous solutions at temperatures between 100 and 360°C. Geochim. Cosmochim. Acta **53**, 313-318.

Wood S., Crerar D.A. and Borcsik M.P. (1987) Solubility of the assemblage pyrite-pyrrhotite-magnetite-sphalerite-galena-gold-stibnite-bismuthinite-argentite-molybdenite in H_2O-NaCl-CO_2 solutions from 200 to 350°C. Econ. Geol. **82**, 1864-1887.

Wood S.A., Samson I.M. (1998) Solubility of ore minerals and complexation of ore metals in hydrothermal solutions. Rev. Econ. Geol. **10**, 33-77.

Yamaguchi T., Johansson G., Holmberg B., Maeda M., Ohtaki H. (1984a) The coordination and complex formation of silver(I) in aqueous perchlorate, nitrate, and iodide solutions. Acta Chem. Scand. **38A**, 437-451.

Yamaguchi T., Lindquist O., Boyce J.B., Claeson T. (1984b) Determination of the hydration structure of silver ions in aqueous silver perchlorate and nitrate solutions from EXAFS using synchrotron radiation. Acta Chem. Scand. **38A**, 423-428.

Yardley B.W. (2005) Metal concentrations in crustal fluids and their relationship to ore formation. Econ. Geol. **100**, 613-632.

Zabinsky S.I., Rehr J.J., Ankudinov A., Albers R.S., Eller M.J. (1995) Multiple scattering calculations of X-ray absorption spectra. Phys. Rev. B **52**, 2995-3009.

Zajacz Z., Halter W.E., Pettke T., Guillong M. (2008) Determination of fluid/melt partition coefficients by LA-ICPMS analysis of co-existing fluid and silicate melt inclusions: Controls on element partitioning. Geochim. Cosmochim. Acta **72**, 2169-2197.

Zajacz Z., Seo J.H., Candela P.A., Piccoli P.M., Tossell J.A. (2011) The solubility of copper in high-temperature magmatic vapors: A quest for the significance of various chloride and sulfide complexes. Geochim. Cosmochim. Acta **75**, 2811-2827.

Zotov A.V., Kudrin A.V., Levin K.A., Shikina N.D., and Var'yash L.N. (1995) Experimental studies of the solubility and complexing of selected ore elements (Au, Ag, Cu, Mo, As, Sb, Hg) in aqueous solutions. in: Shmulovich, K.I, Yardley, B.W.D., Gonchar, G.G. (Eds.), Fluids in the Crust. Equilibrium and Transport Properties, Chapman & Hall, London, pp. 95-138.

Table 1. Silver dissolved concentrations derived from the absorption edge step [(a)], and Ag(I) local structure derived from EXAFS spectra at Ag K-edge [(b)] of nitrate and chloride aqueous solutions investigated in this study.

T, °C	P, bar	m_{Ag}, mol/kg H_2O	atom	N, atoms	R, Å	σ^2, Å^2	c_3, Å^3	$\mathcal{R}$-factor
# 1: 0m total Cl, 0.21m $AgNO_3$-0.10m HNO_3-0.10m H_2O_2								
30	600	0.21±0.01	O	6.0	2.34	0.020	< 0.0003	0.003
100	600	0.21±0.02	O	5.5	2.32	0.020	< 0.0003	0.006
200	630	0.21±0.02	O	4.8	2.30	0.020	< 0.0003	0.010
			error	±1.5	±0.02	±0.005	±0.0003	
# 6: 0.70m total Cl, 0.17m AgCl-0.42m NaCl-0.11m HCl-0.06m H_2O_2								
200	600	0.0074±0.0005	Cl	nd	nd	nd	nd	nd
300	600	0.049±0.003	Cl	1.8	2.38	0.005	0.0007	0.011
400	750	0.14÷0.12	Cl	1.9	2.38	0.007	0.0005	0.010
450	750	0.11÷0.08	Cl	1.9	2.37	0.007	0.0005	0.008
# 2-4: 2.6m total Cl, 0.18m AgCl-2.34m NaCl-0.12m HCl-0.06m H_2O_2								
200	600	0.047±0.003	Cl	2.1	2.47	0.009	0.0012	0.008
300	630	0.20÷0.15	Cl	1.9	2.43	0.009	0.0009	0.009
400	600	0.15÷0.13	Cl	1.9	2.40	0.008	0.0005	0.007
# 5: 5.9m total Cl, 0.30m AgCl-5.51m NaCl-0.14m HCl-0.07m H_2O_2								
200	600	0.16±0.02	Cl	2.5	2.49	0.012	0.0008	0.015
300	620	0.33±0.03	Cl	2.1	2.47	0.011	0.0012	0.009
400	630	0.29±0.03	Cl	1.9	2.44	0.010	0.0010	0.009
450	640	0.28±0.03	Cl	1.8	2.42	0.010	0.0007	0.010
			error	±0.2	±0.01	±0.003	±0.0004	

(a) Dissolved Ag concentrations were determined from the amplitude of the absorption edge height of transmission spectra ($\Delta\mu$) based on the classical X-ray absorption relation (see for details Pokrovski et al., 2005a, 2006, 2009a,b; Testemale et al., 2005): $C_{Ag} = \Delta\mu / (\Delta\sigma_{Ag} \times M_{Ag} \times l \times d_{fluid})$, where C_{Ag} is Ag aqueous concentration (mol kg^{-1} of fluid), $\Delta\sigma_{Ag}$ is the change of the total absorption cross-section of Ag over its K-edge (45.865 cm^2 g^{-1}), l is the optical path length inside the cell (0.40 cm) which remains constant through the experiment, M_{Ag} is Ag atomic weight (0.1079 kg mol^{-1}), and d_{fluid} is the density of the aqueous solution (g cm^{-3}) at given T and P, estimated using the densities of NaCl-H_2O fluids (Bakker, 2003), and assuming that AgCl/HCl/H_2O_2 solutes in water yield the same contribution to the fluid density as the equivalent weight concentration of NaCl. Uncertainties on Ag concentration stem from those of the determination of $\Delta\mu$, l and d_{fluid} (see Pokrovski et al., 2005a, 2009a for details), and minor losses from solution due to $AgCl_{(s)}$ precipitation. Values of m_{Ag} in italic show significant change with time owing to precipitation of AgCl in the cell colder zones; they were not considered in the solubility analyses.

(b) R = Ag-O/Cl mean distance, N = Ag coordination number, σ^2 = squared Debye-Waller factor (relative to $\sigma^2 = 0$ adopted in the calculation of reference amplitude and phase functions by FEFF); c_3 = third-order cumulant accounting for weak anharmonicity in the distance distribution; $\mathcal{R}$-factor defines goodness of the total fit in R-space, which is a fractional misfit between the data and model: $\mathcal{R}=\Sigma(\text{data-model})^2/\Sigma\text{data}^2$. For all samples the fitted R-ranges are 1.1-2.8 Å (not corrected for phase shift), and k-ranges are 2.5-10.0 Å^{-1} and 3.0-11.8 Å^{-1} for nitrate and chloride solutions, respectively (except exp #6 at 300°C, which was recorded to 8 Å^{-1}). The value of Δe, which is a non-structural parameter accounting for phase shift between experimental spectrum and FEFF calculation, is 3.5±0.5 eV for all spectra. The number of variables in the fit (N_{var} = 4 to 5) was always lower than the number of independent points (N_{ind} ~8) as defined in IFEFFIT (Newville, 2001). nd = not determined because of too weak EXAFS signal.

Table 2. Fraction of high-order silver chloride complexes ($AgCl_3^{2-}$ ± $AgCl_4^{3-}$) in the total dissolved silver in the investigated aqueous solutions as inferred from the number of Cl neighbors and Ag-Cl interatomic distances (Table 1), and its comparison with thermodynamic predictions using available stability constants for Ag chloride species.

m_{Cl} mol/kg H_2O	T°C	% [$AgCl_3$] from N_{Cl} (a)	% [$AgCl_3$] from R_{Cl} (b)	% $AgCl_3^{2-}$ Zot95 (c)	% $AgCl_3^{2-}$ + $AgCl_4^{3-}$ Sve97 (d)	% $AgCl_3^{2-}$ Sew76 (e)
0.7	300	< 20	< 10	12	13	7
0.7	400	< 20	< 10	< 5	16	na
0.7	450	< 20	< 10	< 1	48	na
2.6	200	< 30	41	44	55	56
2.6	300	< 20	23	15	62	38
2.6	400	< 20	9	6	94	na
5.9	200	50	50	65	80	73
5.9	300	< 20	41	29	86	60
5.9	400	< 20	27	16	99	na
5.9	450	< 20	18	< 10	> 99	na
error		±20	±15	±10	±7	±5

(a) From average N_{Cl} value ±0.2 Cl atoms (experimental EXAFS, this study, Table 1)
(b) From average R_{Cl} value ±0.01 Å (Table 1) and adopting Ag-Cl distances of 2.38±0.01 Å (experimental EXAFS, this study) and 2.60±0.05 Å (FPMD calculations, this study) for $AgCl_2^-$ and $AgCl_3^{2-}$, respectively.
(c) Using the HKF parameters of Ag^+, $AgCl^0$ and $AgCl_2^-$ from Akinfiev and Zotov (2001), which yield identical stability constants for these species as older works of the same group (Zotov et al., 1995; Tagirov et al., 1997), and using the stability constants of $AgCl_3^{2-}$ reported in Zotov et al. (1995) to 350°C at P_{sat}. Because AgCl solubility data (Zotov et al., 1995; Tagirov et al, 1997) indicate a negligible effect of pressure on the solubility at T to at least 350°C and P to 500-1000 bar, the $AgCl_3^{2-}$ stability constants at P_{sat} were assumed to be the same at our experimental pressure of ~600 bar. See Pokrovski et al. (2009a) for details on thermodynamic data for other fluid constituents and activity coefficient models.
(d) Sverjensky et al. (1997) using the HKF parameters for [$AgCl_{1-4}$] complexes.
(e) Seward (1976) reported stability constants of $AgCl_3^{2-}$ to 200°C at P_{sat}. We extrapolated according to his data the equilibrium constant of the pseudo-isocoulombic reaction $AgCl_2^- + Cl^- = AgCl_3^{2-}$ versus 1/T(K) to 300°C and assumed that this constant is independent of pressure to at least 600 bars.
na = not applicable because requires too far extrapolations on temperature.

Table 3. Thermodynamic properties of silver chloride complexes from the literature, recommended on the basis of XAS analyses, FPMD simulations, and in-situ XAS measured AgCl(s) solubility of this study.

Species	Thermodynamic data	References
Ag^{+} [(d)]	G [(a)] = 18427 cal/mol, S[(b)] = 17.54 cal/(mol K), HKF model coefficients: $a_1 \times 10$ = 1.7285 cal/(mol bar), $a_2 \times 10^{-2}$ = -3.5608 cal/mol, a_3 = 7.1496 cal K/(mol bar), $a4 \times 10^{-4}$ = -2.6318 cal K/mol, c_1 = 18.8783 cal/(mol K), $c_2 \times 10^{-4}$ = -4.4327 cal K/mol, $\omega \times 10^{-5}$ = 0.2160 cal/mol	Akinfiev and Zotov, 2001
$AgCl^0(aq)$ [(d)]	G = -17399 cal/mol, S = 32.067 cal/(mol K), HKF model coefficients: $a_1 \times 10$ = 4.2750 cal/(mol bar), $a_2 \times 10^{-2}$ = 3.7555 cal/mol, a_3 = 4.2739 cal K/(mol bar), $a4 \times 10^{-4}$ = -2.9343 cal K/mol, c_1 = 3.0441 cal/(mol K), $c_2 \times 10^{-4}$ = -4.1199 cal K/mol, $\omega \times 10^{-5}$ = 0.00 cal/mol	Akinfiev and Zotov, 2001
$AgCl_2^-$	G = -51350 cal/mol, S = 49.78 cal/(mol K), HKF model coefficients: $a_1 \times 10$ = 7.1327 cal/(mol bar), $a_2 \times 10^{-2}$ = 9.8065 cal/mol, a_3 = 1.8947 cal K/(mol bar), $a4 \times 10^{-4}$ = -3.1844 cal K/mol, c_1 = 4.8953 cal/(mol K), $c_2 \times 10^{-4}$ = -6.7789 cal K/mol, $\omega \times 10^{-5}$ = 0.6667 cal/mol	Akinfiev and Zotov, 2001
$AgCl_3^{2-}$	Reaction $AgCl(s) + 2Cl^- = AgCl_3^{2-}$ $\log_{10}K = -2230.4/T(K) + 4.391 - 0.00528\ T(K)$ (P_{sat}, 293-648 K) [(c)]	Zotov et al., 1995
Chlorargirite, AgCl(s)	G = -26247 cal/mol, S = 22.99 cal/(mol K), V = 25.727 cm^3/mol, Heat capacity coefficients (cal units): $14.331 + 1.821 \times 10^{-3}\ T(K) - 2.431 \times 10^5/T(K)^2$ (298-728 K)	Robie and Hemingway, 1995

[(a)] G = standard molal Gibbs free energy of formation from the elements at 25°C, 1 bar
[(b)] S = standard molal entropy at 25°C, 1 bar
[(c)] Assumed to be valid to 1000 bar (see footnote of Table 2)
[(d)] These species are included for consistency, but are minor in saline fluids compared to the di- and tri-chloride.

Figure captions

Fig. 1. Distribution of Ag-chloride species in an acidic aqueous solution as a function of NaCl concentration at 400°C and 800 bar, calculated using the thermodynamic properties of silver chloride complexes reported by (a) Sverjensky et al. (1997; SUPCRT 2007, http://geopig.asu.edu/index.html#) and (b) Akinfiev and Zotov (2001), both based on regressions of available experimental data within the framework of the revised HKF model. Thermodynamic data for other fluid constituents and activity coefficient models are detailed in Pokrovski et al. (2009a). Note significant differences in the Ag species distribution at NaCl concentration above 0.5m according to these two main databases largely used by geochemists.

Fig. 2. Solubility of argentite (Ag_2S, cubic) in a model aqueous fluid of 1.5m NaCl + 0.5m KCl (~25 wt% NaCl equivalent) as a function of temperature at 1000 bar in equilibrium with the Pyrite-Pyrrhotite-Magnetite sulfur fugacity buffer and Muscovite(±Andalusite)-Kfeldspar-Quartz acidity buffer, according to the two major thermodynamic datasets for Ag chloride complexes, Sverjensky et al. (1997; SUPCRT http://geopig.asu.edu/index.html#) and Akinfiev and Zotov (2001). Thermodynamic data for other fluid constituents and activity coefficient models are detailed in Pokrovski et al. (2009a). Differences in Ag_2S solubility attain a factor of 10 to 50 between 400 and 600°C. The inflexion of both solubility curves above 500°C is due to the muscovite breakdown to andalusite, which leads to pH increase in the fluid at these conditions.

Fig. 3. (a) Normalized k^2-weighted EXAFS spectra of studied Ag nitrate and chloride solutions at 600-750 bars and indicated temperatures (in °C), and (b) their corresponding Fourier Transform (FT) magnitudes (not corrected for phase shift). Vertical dashed line in (a) is drawn to indicate the phase shift between O and Cl backscattering atoms in nitrate and chloride solutions and temperature changes in Ag-Cl distances in chloride solutions. Vertical dashed lines in (b) indicate approximate positions of O and Cl atoms in the first coordination shell of Ag (see Table 1 for phase-corrected distances).

Fig. 4. Average Ag-Cl distances (a) and number of Cl atoms (b) in the first silver coordination shell derived from EXAFS analyses of chloride aqueous solutions as a function of temperature.

Fig. 5. (a) Normalized XANES spectra at Ag K-edge of selected nitrate and chloride aqueous solutions and solid reference compounds. (b) XANES spectra of representative AgO/Cl clusters of different stoichiometry and geometry, calculated using the FDMNES code (Joly, 2001). Vertical lines on both panels indicate the major spectral features discussed in section 3.2.

Fig. 6. Comparison of calculated XANES spectra for the representative Ag-Cl clusters of different geometry and degree of distortion with key experimental spectra: (a) $AgCl_2$ clusters ($R_{Ag\text{-}Cl}$= 2.35 Å) with different Cl-Ag-Cl angles (in degrees in the figure legend) versus the experimental spectrum of the most dilute Cl solution at 450°C (exp6_0.70m Cl); (b) $AgCl_3$ ($R_{Ag\text{-}Cl}$ = 2.55 Å) and $AgCl_4$ clusters (R_{AgCl} mean ~ 2.50 Å, ΔR in the figure legend indicates the difference between two pairs of Ag-Cl distances in the distorted tetrahedral-like cluster).

Fig.7. Structures of stable Ag-Cl-O species identified by FPMD simulations with Ag-Cl interatomic distances (in Å) and Cl-Ag-Cl angles (in degrees): (a) $AgCl(H_2O)$, (b) $AgCl_2^-$, (c) $AgCl_3^{2-}$, d) $AgCl_3(H_2O)^{2-}$, and e) $AgCl_4^{3-}$.

Fig. 8. Local environment of the $AgCl_2^-$ species derived from FPMD simulations at 50°C, 1 bar and 380°C, 600 bar (with Cl:Ag ratio = 2 in the system). (a) Ag-Cl and Ag-O radial distribution functions, and (b) Cl-Ag-Cl angular distributions. The amplitude of the Ag-Cl radial distribution functions in (a) is divided by 60 to allow comparison with that of Ag-O.

Fig. 9. Comparison of the MD-EXAFS spectrum of the $AgCl_2^-$ species at 380°C, 600 bar with the experimental spectrum obtained from 0.7m Cl solution at 400°C, 750 bar (exp#6). The MD calculated spectrum was scaled by 0.75 in amplitude (experimental amplitude reduction factor) and shifted along the k axis (non-structural Δe value in EXAFS, see text) for better comparison.

Fig. 10. MD-EXAFS spectra of (a) $AgCl_2^-$ at 50°C/1 bar and 380°C/600 bar, and (b) $AgCl_2^-$, $AgCl_3^{2-}$, and $AgCl_4^{3-}$ at 50°C/1 bar. The $AgCl_3(H_2O)^{2-}$ spectrum (not shown) is close to that of $AgCl_4^{3-}$. Note the strong similarity of the spectra of $AgCl_2^-$ and $AgCl_4^{3-}$ (see text).

Fig. 11. Solubility of AgCl(s) at 200°C and 600 bars measured in situ from the absorption edge height of transmission spectra in this study (symbols) and its comparison with values calculated using available thermodynamic data for Ag chloride complexes. The uncertainties of XAS measurements are comparable with the symbol size. Aki01 – Akinfiev and Zotov (2001) for $AgCl^0$ and $AgCl_2^-$; Zot95 – Zotov et al. (1995) for $AgCl_3^{2-}$; Sew76 – Seward (1976) for $[AgCl_{1-3}]$ complexes; Sve97 – Sverjensky et al. (1997) for $[AgCl_{1-4}]$ complexes.

Fig. 12. Solubility of argentite, native gold, and chalcopyrite (a) as a function of temperature in a model aqueous solution of 10 wt% NaCl equivalent at pH 5 in equilibrium with the pyrite-magnetite-hematite oxygen and sulfur fugacity buffer at pressures progressively decreasing from 1500 bar at 450-550°C to 200 bar below 250°C; b) as a function of pH at 400°C, 500 bar, 10 wt% NaCl, in equilibrium with pyrite-magnetite-hematite; c) as a function of salinity at 400°C, 500 bar, pH 5, in equilibrium with pyrite-magnetite-hematite; d) as a function of H_2S concentration at 400°C, 500 bar, 10 wt% NaCl, pH 5, and oxygen fugacity of the magnetite-hematite buffer. Calculations were performed using the HCh computer code (Shvarov, 2008). Thermodynamic properties of the minerals are taken from SUPCRT (Johnson et al., 1992), those of major fluid constituents and activity coefficient models are detailed in Pokrovski et al. (2009a,b). Stability constants of Ag, Cu, and Au aqueous chloride and sulfide complexes are from Zotov et al. (1995) for $AgCl_3^{2-}$, Akinfiev and Zotov (2001) for $AgCl_2^-$ and $CuCl_2^-$, Akinfiev et al. (2008) for AgHS, $Ag(HS)_2^-$, CuHS, $Cu(HS)_2^-$, AuHS, and $Au(HS)_2^-$, and Pokrovski et al. (2009a) for $AuHS(H_2S)$. These thermodynamic datasets are in good agreement with the major experimental data sources. The dominant aqueous species for each metal are indicated.

Figure 1

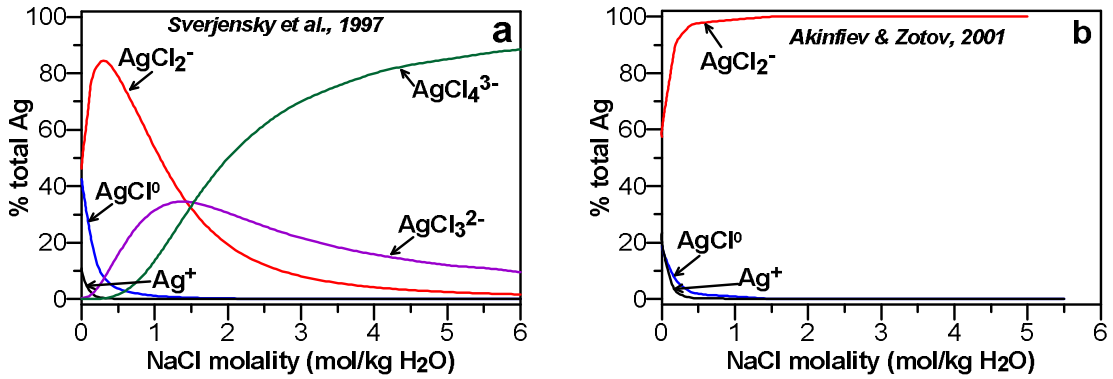
Sverjensky et al., 1997
a
AgCl2-
AgCl43-
AgCl0
AgCl32-
Ag+
% total Ag
NaCl molality (mol/kg H2O)
Akinfiev & Zotov, 2001
b
AgCl2-
AgCl0
Ag+
% total Ag
NaCl molality (mol/kg H2O)

Figure 2

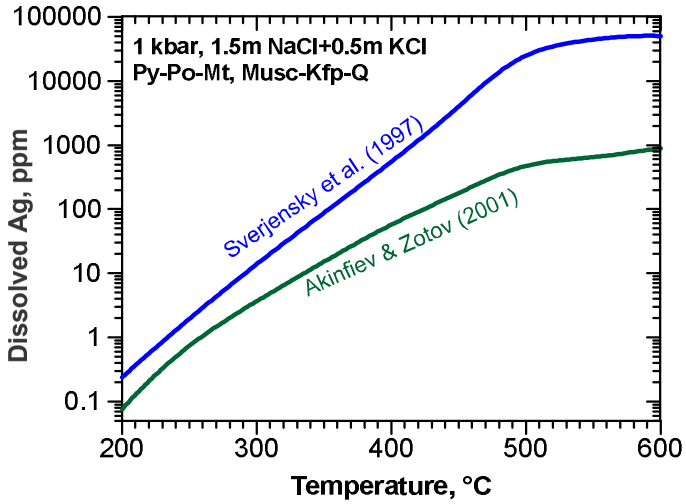
1 kbar, 1.5m NaCl+0.5m KCl
Py-Po-Mt, Musc-Kfp-Q
Sverjensky et al. (1997)
Akinfiev & Zotov (2001)
Dissolved Ag, ppm
100000
10000
1000
100
10
1
0.1
200
300
400
500
600
Temperature, °C

Figure 3

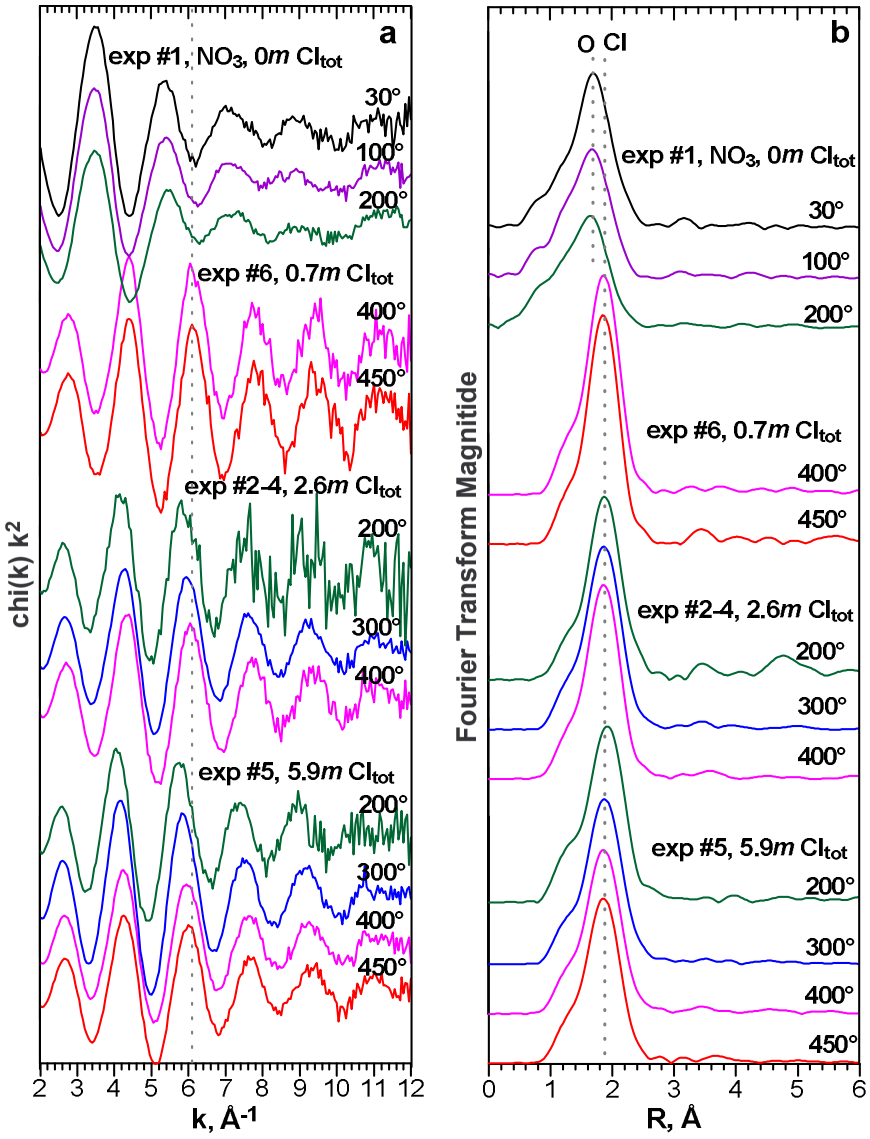
a
exp #1, NO3, 0m Cltot
30°
100°
200°
exp #6, 0.7m Cltot
400°
450°
exp #2-4, 2.6m Cltot
200°
300°
400°
exp #5, 5.9m Cltot
200°
300°
400°
450°
chi(k) k2
k, Å-1
b
O Cl
exp #1, NO3, 0m Cltot
30°
100°
200°
exp #6, 0.7m Cltot
400°
450°
exp #2-4, 2.6m Cltot
200°
300°
400°
exp #5, 5.9m Cltot
200°
300°
400°
450°
Fourier Transform Magnitide
R, Å

Figure 4

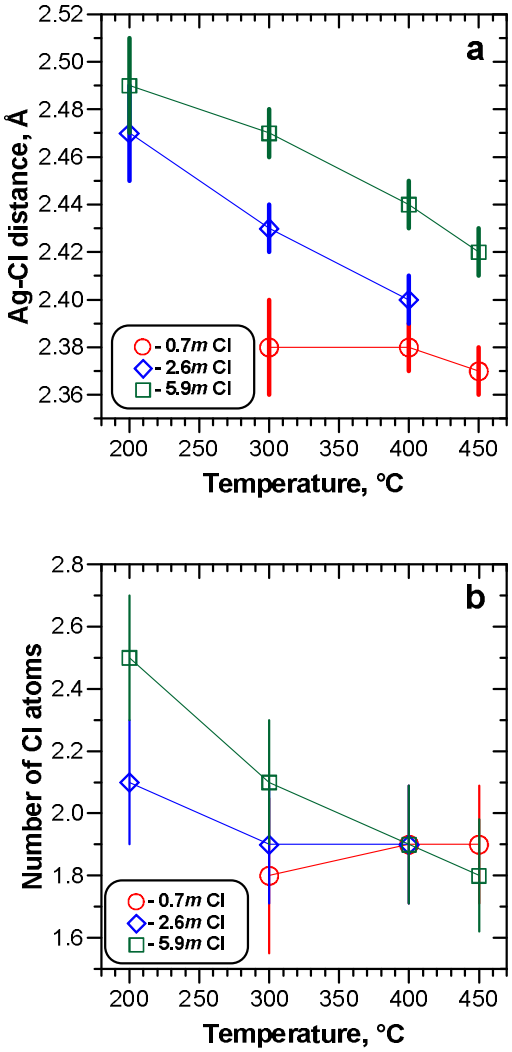
a
Ag-Cl distance, Å
2.52
2.50
2.48
2.46
2.44
2.42
2.40
2.38
2.36
200
250
300
350
400
450
Temperature, °C
- 0.7m Cl
- 2.6m Cl
- 5.9m Cl
b
Number of Cl atoms
2.8
2.6
2.4
2.2
2.0
1.8
1.6
200
250
300
350
400
450
Temperature, °C
- 0.7m Cl
- 2.6m Cl
- 5.9m Cl

Figure 5

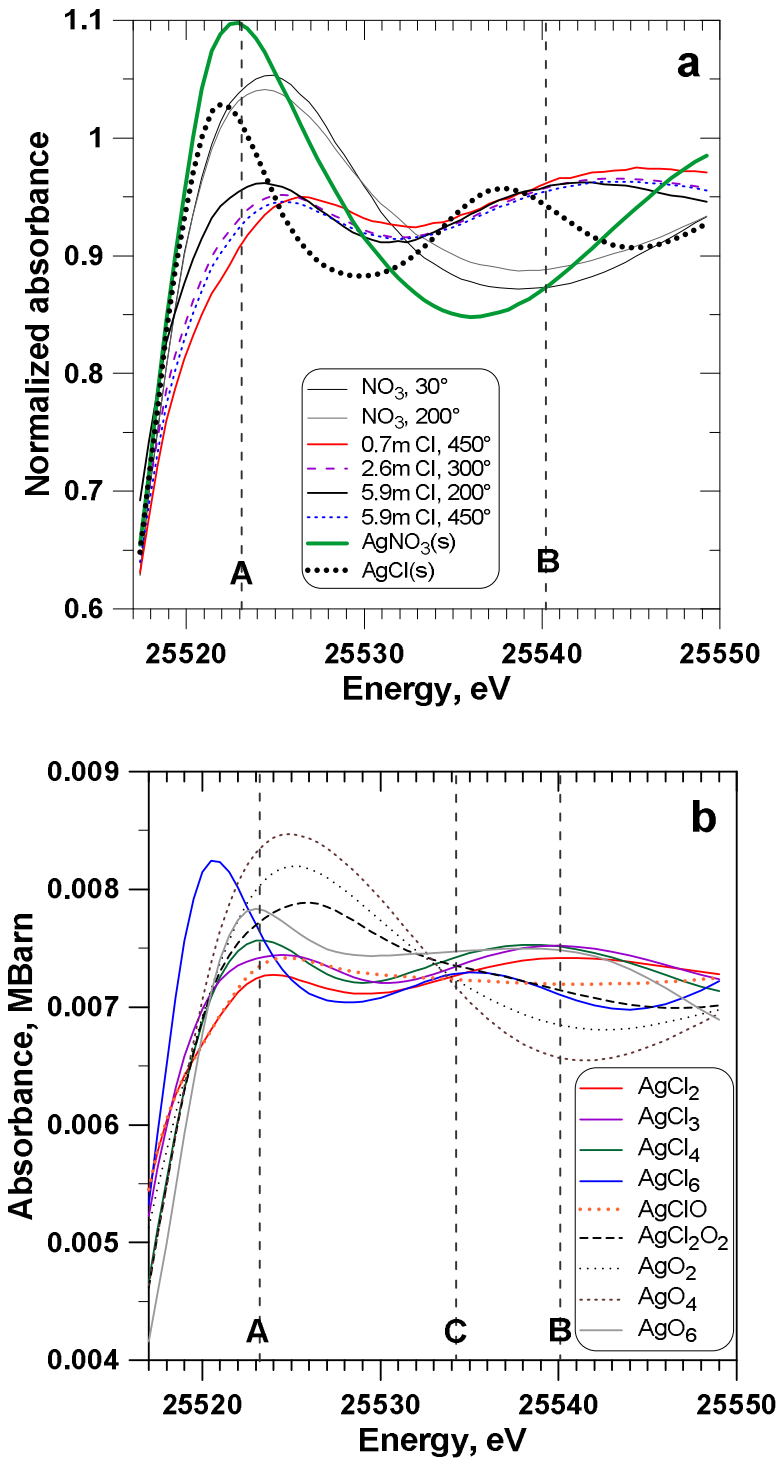
a
Normalized absorbance
Energy, eV
1.1
1
0.9
0.8
0.7
0.6
25520
25530
25540
25550
A
B
NO3, 30°
NO3, 200°
0.7m Cl, 450°
2.6m Cl, 300°
5.9m Cl, 200°
5.9m Cl, 450°
AgNO3(s)
AgCl(s)
b
Absorbance, MBarn
0.009
0.008
0.007
0.006
0.005
0.004
A
C
B
AgCl2
AgCl3
AgCl4
AgCl6
AgClO
AgCl2O2
AgO2
AgO4
AgO6

Figure 6

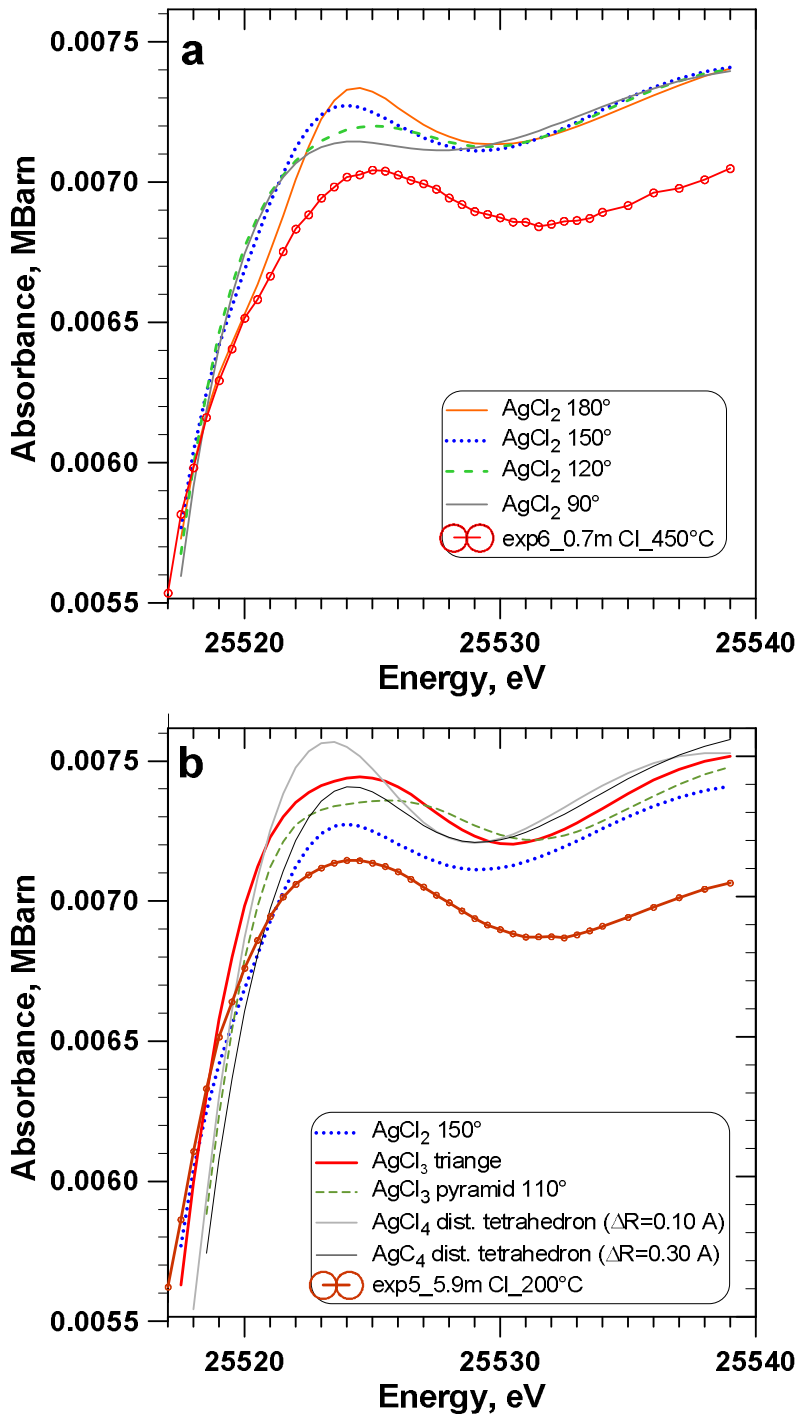
a
0.0075
0.0070
0.0065
0.0060
0.0055
Absorbance, MBarn
25520
25530
25540
Energy, eV
AgCl2 180°
AgCl2 150°
AgCl2 120°
AgCl2 90°
exp6_0.7m Cl_450°C
b
0.0075
0.0070
0.0065
0.0060
0.0055
Absorbance, MBarn
25520
25530
25540
Energy, eV
AgCl2 150°
AgCl3 triange
AgCl3 pyramid 110°
AgCl4 dist. tetrahedron (ΔR=0.10 A)
AgC4 dist. tetrahedron (ΔR=0.30 A)
exp5_5.9m Cl_200°C

Figure 7

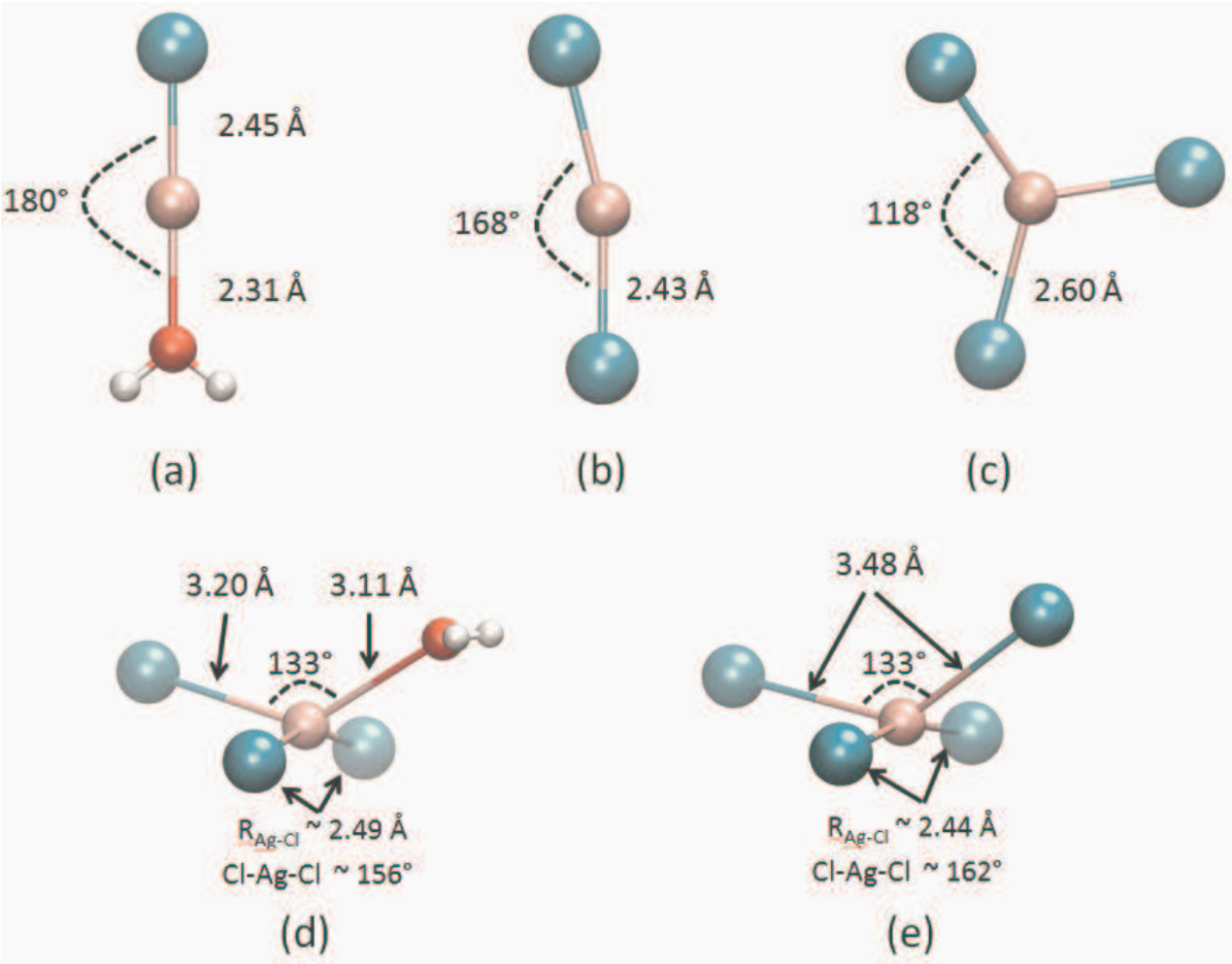
2.45 Å
180°
2.31 Å
(a)
168°
2.43 Å
(b)
118°
2.60 Å
(c)
3.20 Å
3.11 Å
133°
R_Ag-Cl ~ 2.49 Å
Cl-Ag-Cl ~ 156°
(d)
3.48 Å
133°
R_Ag-Cl ~ 2.44 Å
Cl-Ag-Cl ~ 162°
(e)

Figure 8

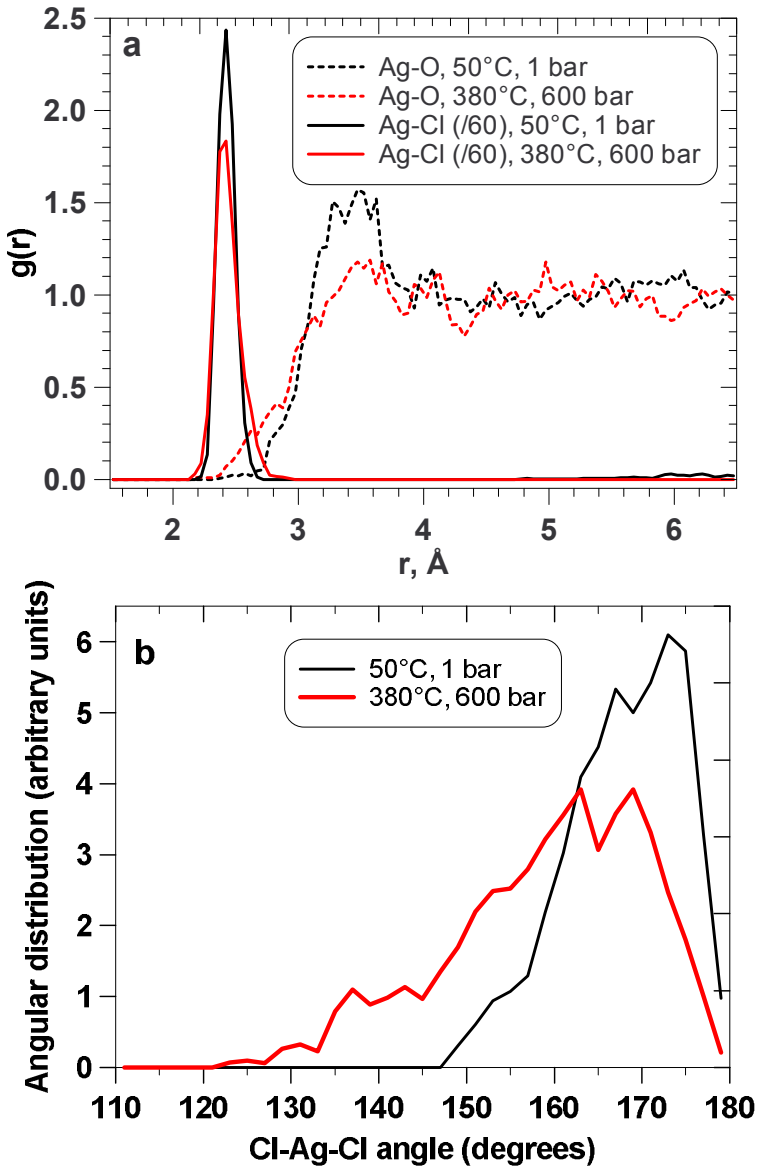
a
Ag-O, 50°C, 1 bar
Ag-O, 380°C, 600 bar
Ag-Cl (/60), 50°C, 1 bar
Ag-Cl (/60), 380°C, 600 bar
g(r)
r, Å
b
50°C, 1 bar
380°C, 600 bar
Angular distribution (arbitrary units)
Cl-Ag-Cl angle (degrees)

Figure 9

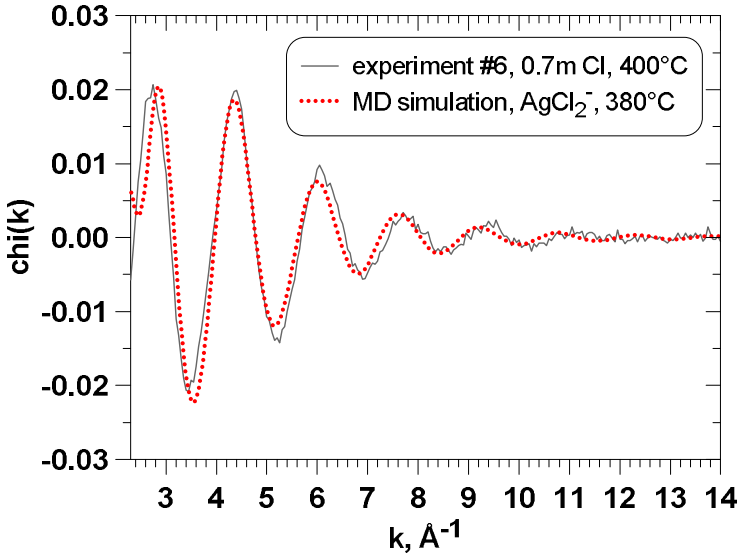
0.03
0.02
0.01
0.00
-0.01
-0.02
-0.03
chi(k)
3
4
5
6
7
8
9
10
11
12
13
14
k, Å-1
experiment #6, 0.7m Cl, 400°C
MD simulation, AgCl2-, 380°C

Figure 10

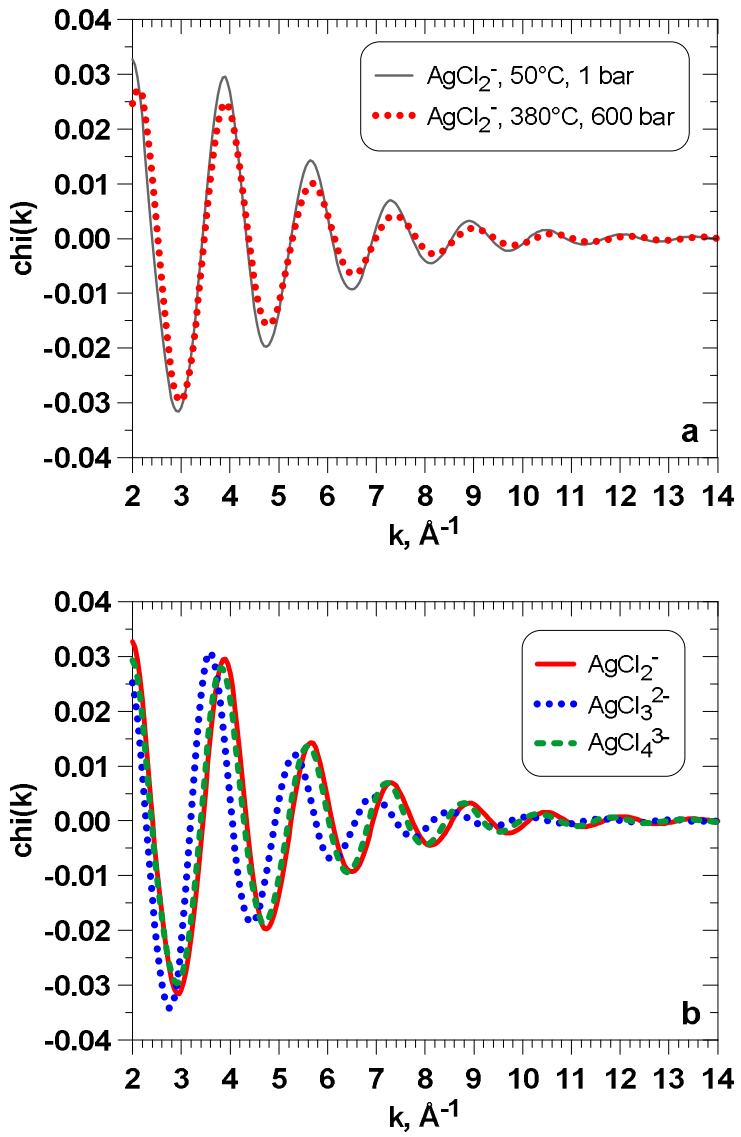
0.04
0.03
0.02
0.01
0.00
-0.01
-0.02
-0.03
-0.04
chi(k)
AgCl2-, 50°C, 1 bar
AgCl2-, 380°C, 600 bar
a
2 3 4 5 6 7 8 9 10 11 12 13 14
k, Å-1
AgCl2-
AgCl32-
AgCl43-
b

Figure 11

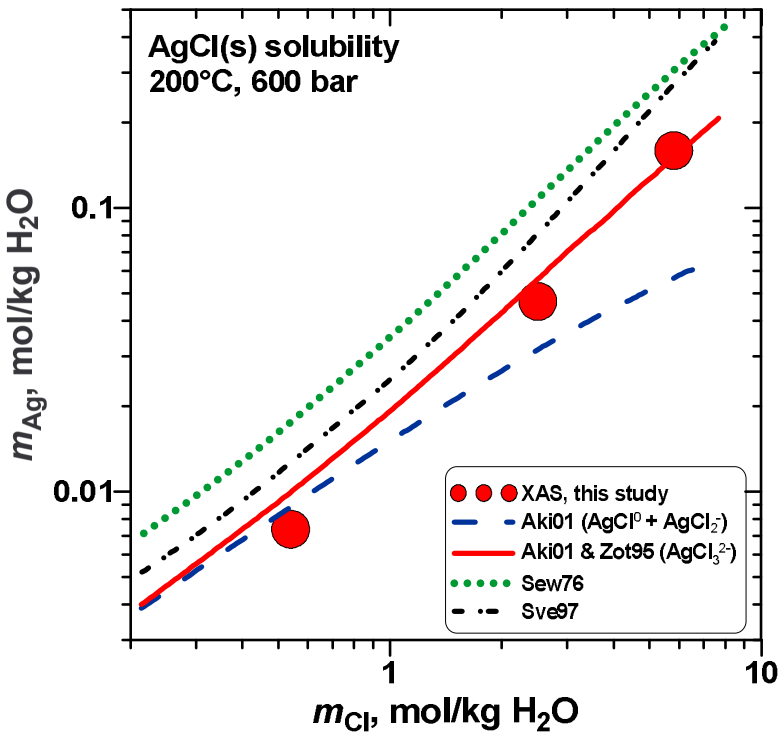
AgCl(s) solubility
200°C, 600 bar
0.1
0.01
1
10
m_{Ag}, mol/kg H_2O
m_{Cl}, mol/kg H_2O
XAS, this study
Aki01 ($AgCl^0$ + $AgCl_2^-$)
Aki01 & Zot95 ($AgCl_3^{2-}$)
Sew76
Sve97

Figure 12

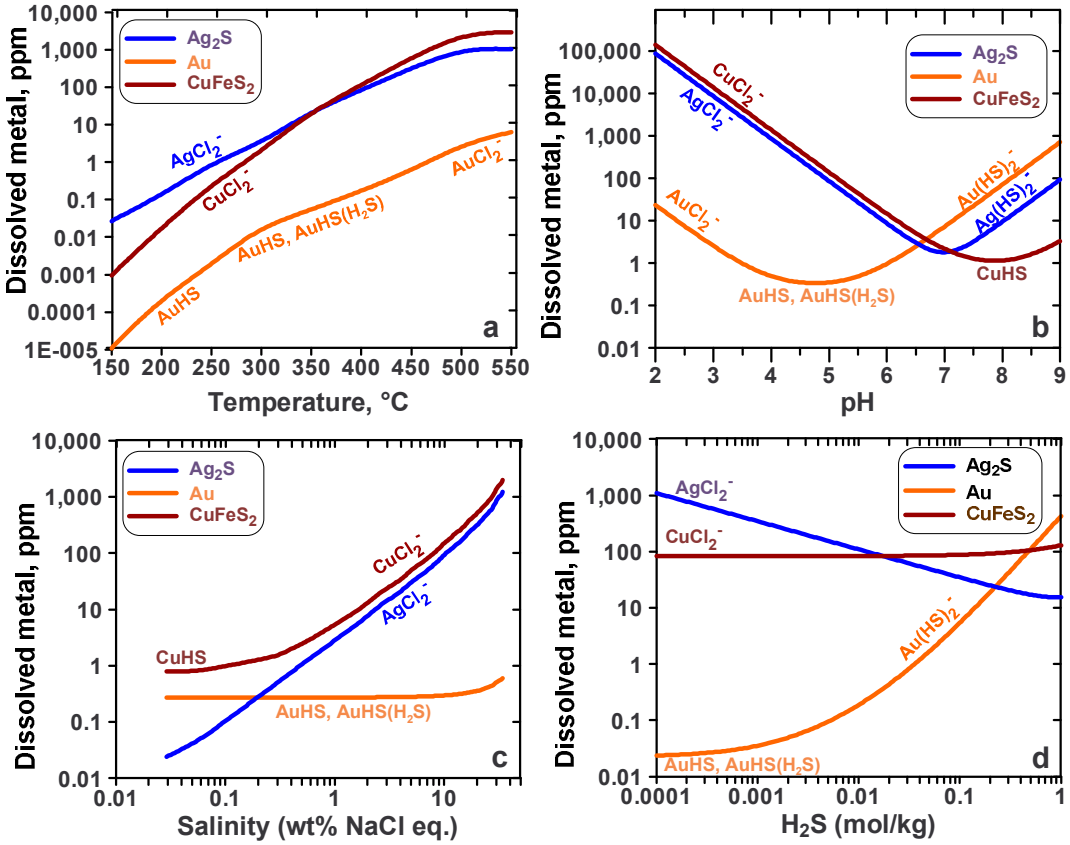
Dissolved metal, ppm
Temperature, °C
Ag2S
Au
CuFeS2
AgCl2-
CuCl2-
AuCl2-
AuHS, AuHS(H2S)
AuHS
a
pH
AuCl2-
Au(HS)2-
Ag(HS)2-
CuHS
b
Salinity (wt% NaCl eq.)
c
H2S (mol/kg)
d

Electronic Annex
Click here to download Electronic Annex: ElectronicAnnex_revised_nov12.pdf